Bipolar electrochemistry

Laurent Bouffier, Dodzi Zigah, Neso Sojic, Alexander Kuhn

Bipolar electrochemistry

Laurent Bouffier, Univ. Bordeaux, ISM CNRS UMR 5255, Bordeaux INP, ENSCBP, 16 avenue Pey Berland, 33607 Pessac, France
Dodzi Zigah, Univ. Bordeaux, ISM CNRS UMR 5255, Bordeaux INP, ENSCBP, 16 avenue Pey Berland, 33607 Pessac, France
Neso Sojic, Univ. Bordeaux, ISM CNRS UMR 5255, Bordeaux INP, ENSCBP, 16 avenue Pey Berland, 33607 Pessac, France
Alexander Kuhn*, Univ. Bordeaux, ISM CNRS UMR 5255, Bordeaux INP, ENSCBP, 16 avenue Pey Berland, 33607 Pessac, France, kuhn@enscbp.fr

Bipolar electrochemistry is a technique that involves two opposite chemical processes, namely an oxidation and a reduction, occurring simultaneously on the surface of a conducting object, usually without connection to a power supply. The basic phenomenon has already been described and used for many decades but regained a lot of interest in recent years, thanks to several attractive features for developing new applications in various areas ranging from materials science and analytical chemistry to catalysis and even life science. Consequently, bipolar electrochemistry has experienced a substantial growth in the number of users and publications. This is mostly due to several advantages over classic electrochemistry, such as the absence of an ohmic contact, the generation of a directional gradient of electroactivity on the object, and the possibility to address simultaneously thousands of objects, which opens the door for high throughput screening of (electro)chemical properties. Also, some features of this “wireless” electrochemistry allow performing experiments that cannot be achieved with a classic electrochemical set-up. Last but not least, only rather low-cost equipment is needed.
The objective of the present contribution is to introduce first some fundamental aspects of bipolar electrochemistry, and then to illustrate its different developments, highlighting not only the historic landmark achievements, but also the most recent findings, especially in the context of micro- and nanoscience. The chapter will illustrate the singularities and advantages of this straightforward approach and hopefully convince the reader of the power of this interesting electrochemical concept.

Bipolar Electrochemistry; Material Science; Analytical Chemistry; Catalysis; Electrochemiluminescence

1. Introduction

When opening electrochemical textbooks, the reader is obviously finding exhaustive theoretical and experimental descriptions of major concepts, which constitute the basis of classic electrochemical techniques such as cyclic voltammetry, chronoamperometry, or coulometry. Most of these latter use a conventional three-electrode set-up, for which working, counter, and reference electrodes are directly connected to a power supply (1). In this case, the protagonist is the working electrode, where either oxidation or reduction reactions are taking place in a controlled way, depending on the potential applied to it with respect to the reference electrode. The counter electrode, having opposite polarity, is physically separated from the working electrode. Also, the redox reactions occurring at the counter electrode are usually not considered in detail.

In contrast to this, bipolar electrochemistry (BPE) deals with a (semi)conducting object on which oxidation and reduction reactions occur simultaneously. The so-called bipolar electrode (BE) does not need to be connected to a power supply, because the driving force of the overall reaction is provided by the polarization of the object with respect to the solution potential. In turn, the solution potential is governed by an electric field imposed by two feeder (or driving) electrodes. As the conducting object is by definition equipotential, the potential gradient in the surrounding solution will lead to a gradually changing potential difference between the solution and the object along its main axis, oriented parallel with respect to the electric field lines. If this polarisation is strong enough, one extremity of the object will be able to drive oxidation processes, whereas the opposite extremity will be the site of reduction reactions. The resulting inhomogeneous reactivity intrinsically constitutes a straightforward strategy for breaking the symmetry in electrochemical systems. Obviously, the basic concept itself is not new, and several important fundamental and applied studies date back to the middle of the last century (2-4). Nevertheless, several intrinsic virtues of this approach were largely underestimated until the beginning of the 21st century. Since then, scientists have discovered new and exciting aspects of BPE, with applications in various areas, ranging from materials science and analytical chemistry to catalysis, energy storage (5-14), and even life science (15).

The possibility of addressing with one single pair of feeder electrodes several thousands or even millions of BEs over the distance is certainly one of the most important intrinsic advantages of the concept. This has been nicely illustrated by early seminal contributions from Fleischmann and collaborators, dealing with the behaviour of dispersions of bipolar microelectrodes (16, 17). It allows carrying out experiments that are simply impossible with more classic electrochemical set-ups. This idea has been a considerable extension with respect to other approaches, using BEs with a different philosophy, for example for stacks in bipolar reactors (18), bipolar batteries (19, 20) or fuel cells (21, 22), as well as in electrolysers (23-25).

The work of Fleischman has then be pushed further in the frame of a series of original contributions by Bradley's group at the turn of the century (26-30). They provided evidence that contemporary BPE opens unexpected perspectives with respect to the controlled generation of hybrid objects at the micro- and nanometer scale. These pioneering experiments have paved the way for a myriad of other remarkable, and sometimes completely unconventional, developments over the last two decades, which can be considered now as milestones in the history of BPE. Some of them will be discussed in the frame of this chapter, others have been summarized in a long series of review articles, books, and a topical journal issue (5-11, 31-37). The interested reader is invited to have a look at these references or other primary literature for further and more detailed information about specific subtopics of BPE. The global objective here is to present BPE as an appealing and quite general concept to a broad audience of scientists, in order to illustrate how this type of approach allows carrying out experiments that are unique and often impossible to perform in other ways.

2. Theory of BPE

2.1. Open configuration

Bipolar behaviour can actually occur spontaneously in a variety of physico-chemical systems, some of them being rather ubiquitous, such as corrosion. Many non-noble metals like iron, nickel, zinc etc. get spontaneously oxidized in aqueous solutions, and the corresponding electrons are used on the same object to reduce oxygen or protons for reasons of charge compensation. However, the spatial distribution of oxidation and reduction spots is rather unpredictable, as can be seen for example in the case of pitting corrosion. In this case, no external electric driving force is necessary to observe bipolar behaviour, and these phenomena can be rather classified as classic redox reactions. In the frame of the present chapter, we are not discussing in too much detail such types of spontaneous thermodynamically driven behaviour, but we will mostly focus on systems where an external driving force is necessary to induce BPE. The BE is in this case a conducting object, positioned in a solution in which an electric field is generated by two so-called feeder electrodes. Most importantly, the latter are not in physical contact with the immersed object.

Having an electric field in the solution intrinsically means that there is a gradient of electric potential, the latter being more positive at the feeder anode and more negative at the feeder cathode. If a conducting object, which is by definition equipotential, is placed in this potential gradient, it will experience an inhomogeneous potential difference with respect to the solution, along an axis of the object oriented parallel to the electric field lines (Figure 1a). The extremity facing the feeder anode will be negatively polarized ($\delta-$) by a value η_c, whereas the opposite extremity shows a positive polarization ($\delta+$) of amplitude η_a. A detailed mathematical treatment of this polarization and the resulting local currents can be found in the literature (38), and we only summarize here the most important points.

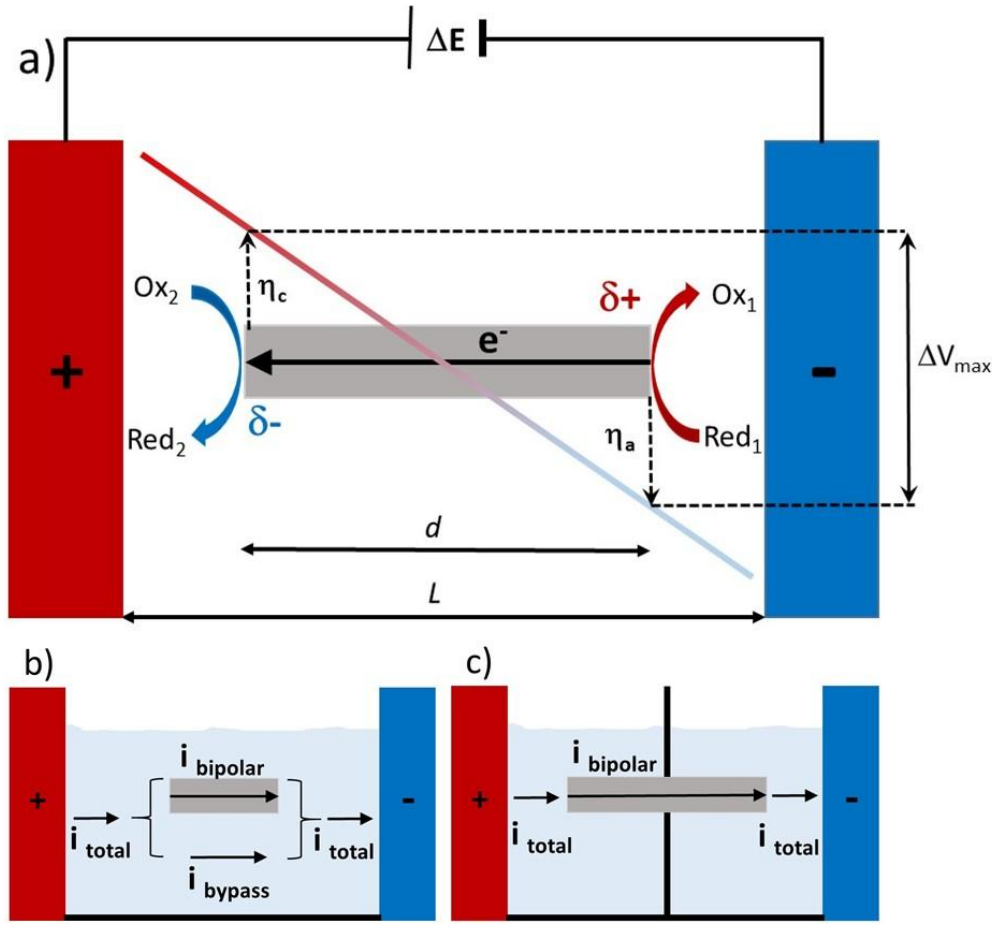

Figure 1. Scheme illustrating the polarization of a bipolar object with respect to the solution potential and the resulting current flow. a) General concept of asymmetric polarization of a conducting object exposed to an electric field in solution. b) Current flow in an open bipolar electrochemical cell. c) Current distribution in a closed bipolar configuration.

Consequently, if the generated overall polarization ($\Delta V_{max} = \eta_a - \eta_c$) is strong enough, some locations at the object's surface are more likely to undergo an oxidation, whereas other parts are more favourable for a reduction reaction, accompanied by a local electron flow through the object. The advantage, compared to the spontaneous bipolar behaviour described above, is that in this scenario the spatial distribution of anodic and cathodic regions, as well as the amplitude of the involved electron transfer reactions, can be perfectly controlled. Thus, BPE is a straightforward mean to trigger an asymmetric and opposite reactivity on the surface of one and the same conducting object in a wireless way. Two fundamentally different ways of conducting BPE experiments can be distinguished and will be discussed in the following.

The more general case is the so-called open configuration, where the bipolar object is completely surrounded by electrolyte and both feeder electrodes are in contact with the very same solution (Figure 1b). In a first order approximation, we can assume that the potential varies linearly throughout the electrolyte. Consequently, the maximum polarization potential difference, established between the two extremities of the object, ΔV_{max}, can be expressed as:

$$\Delta V_{max} = (\Delta E \times d)/L \quad (1)$$

If two electroactive species, Red_1 and Ox_2, which can undergo the following reactions:

$$Red_1 \rightarrow Ox_1 + e^- \quad (2)$$

and

$$Ox_2 + e^- \rightarrow Red_2 \quad (3)$$

are present in solution, they can be transformed at the respective extremities, under the condition that

$$\Delta V_{max} > E^\circ_1 - E^\circ_2 \quad (4)$$

with $E^\circ_1 > E^\circ_2$

From these equations, it becomes immediately clear that for a given couple of redox reactions the possibility of triggering bipolar behaviour depends essentially on the overall electric field in the cell and the characteristic size of the object. Obviously, this might constitute a limitation when trying to carry out BPE on nanoobjects, for which extremely high electric fields are then necessary (up to MV/m). Another possible problem, which is directly related to the open configuration, is the fact that the current cannot only flow through the bipolar object, but also through the electrolyte, as illustrated in Figure 1b. This bypass current i_{bypass} has to be kept to a minimum by using solutions with a rather high resistance compared to the resistance of the BE. Consequently, BPE experiments are often carried out in the absence of supporting electrolyte (or in weakly concentrated supporting electrolyte), an important difference compared to classic electrochemistry.

If this is not possible, an alternative option is to use a so-called closed configuration, discussed in the next section.

2.2. Closed configuration

In a closed set-up, illustrated very schematically in Figure 1c, the BE is the only existing current path between two reservoirs, each of them containing one of the two feeder electrodes. This implies that the BE (or at least a section of the BE) is completely surrounded by an insulator, typically a membrane, actually dividing the cell into two independent compartments. Even though such a set-up is slightly more complicated, it has several important advantages, especially when handling BEs with dimensions in the micro- and nanometer range, for which it becomes an almost mandatory cell design. The total absence of bypass current is an interesting feature, especially for cases where a high faradaic current efficiency is required, e.g. for analytical applications (39). In contrast to the open configuration, almost the entire externally applied potential is forced to drop between the two extremities of the BE, which means that in general a lower global driving force needs to be applied between the feeder electrodes. A direct consequence and advantage of the two independent compartments is the possibility to use completely different solution compositions in the anodic and cathodic half-cells. As the reducing and oxidizing agents are

now physically separated, incompatible reagents, e.g. in terms of solubility, redox potential or pH stability, can be used as partners of the bipolar reaction. If necessary, such a set-up also allows isolating more easily reaction products from the initial reactants in every compartment individually. A slight variation of this concept, where one and the same object is in contact with both half-cells, is to use a so-called split-BE. Two distinct conducting objects, located in the respective, completely isolated compartments, are connected externally via a wire and thus constitute a single BE. Such a set-up not only allows measuring eventually the local current flowing through the BE, but also separating the two reactive extremities of the BE over large distances. This might have important advantages, especially for analytical applications that will be discussed further down.

A special case, which is also a kind of analogue of a closed bipolar configuration, takes advantage of the interface between two immiscible electrolyte solutions (40). Adsorption of 2-dimensional conducting microobjects at such interfaces (41-43) allows addressing them electrochemically and selectively at both sides. By choosing the right composition of the respective solutions, i.e. avoiding the use of ions being able to cross the interface, the majority of the overall current passing through the set-up should be produced exclusively by redox transformations at the interfacial particles.

Another, less common, but very original approach for performing BPE is based on electrokinetic effects. It is neither an open nor a closed configuration, because actually no feeder electrodes are used, and thus no electrode compartments can be defined. It also cannot be considered as a spontaneous bipolar behaviour, based on the combination of two redox couples in a thermodynamically favourable way, as discussed at the beginning of this chapter. In fact, an external driving force still remains necessary and is applied in the form of pressure gradients, inducing liquid flow around the BE. Under certain conditions, mostly governed by the cell configuration and the composition of the electrolyte, streaming potentials are generated based on the Smoluchowski equation (44, 45), which can become sufficient to promote BPE at the extremities of an object exposed to the liquid flow (46). However, the generated polarisation potential differences are usually rather small and it seems quite difficult to extend the use of this approach beyond some exotic cases.

In conclusion of these brief fundamental considerations, the two major configurations of BPE described above have their individual advantages and drawbacks. Therefore, using one or the other will mostly depend on the specific requirements of a given experimental challenge, e.g. whether one wants to address analytical problems, provide efficient means for the large-scale synthesis of asymmetric particles or for example induce the electro-mechanical locomotion of objects. Obviously, all the explanations provided and illustrated so far for a single BE, are also valid for ensembles or arrays of multiple BEs. Addressing simultaneously thousands and eventually millions of BEs with just one pair of feeder electrodes remains one of the key advantages of BPE, as will be illustrated further down with the help of some unique applications of this concept.

2.3. Practical cell designs

From a more practical point of view, carrying out BPE experiments requires very different cell designs, as a function of the envisioned application. The degree of complexity can largely vary, from a simple beaker with two classic electrodes dipping in a standard aqueous electrolyte, to very complex cell architectures with several compartments or channels, sophisticated feeder electrode structures and unusual electrolytes such as for example ionic liquids or jellified solutions.

Historically, bipolar electrochemical cells were often based on BE plates, stacked between a pair of feeder electrodes. The plates themselves can be either plain, perforated or in the extreme case even conducting porous membranes, resulting in either an open or a closed configuration. Another design, that is often adopted for industrial applications, is a bed of individual millimeter or sub-millimeter sized conducting particles (47). They are packed either randomly or in an ordered way, and need to be electrically insulated from each other. This can be achieved by wrapping them into an insulating spacer material, such as a polymer net or mesh. Instead of a static bed of particles, fluidized bed reactors are also often employed in the context of BPE. In this case, the bed is constituted by a suspension of conducting particles, which are maintained in motion, either by stirring or by a continuous stream of electrolyte (48). The resulting high active surface area allows a straightforward scale-up of electrochemical processes (49).

Depending on the type of bipolar reactions that are to be carried out, a major drawback of these cell designs might be the reactions occurring at the feeder electrodes. For example, in the case of bipolar electrodeposition of metals, a certain, sometimes quite important fraction of the metal salt will not only get reduced at the negatively polarized extremity of the BE, but also on the feeder cathode, and is therefore lost. In this case, it is advantageous to introduce membranes that separate the feeder electrodes from the compartment where the BPE occurs (50). Obviously, this will result in a more or less important potential drop across these membranes. However, it will help to decrease the detrimental impact of the feeder electrodes, not only regarding a parasitic transformation of reactant at their surface, but also with respect to other problems that might occur when using intense electric fields, such as bubble formation, solvent evaporation and convection due to ohmic heating. With this configuration, the electric field can be imposed for relatively long periods of time before observing such problems.

In the extreme case, when very high electric fields are needed, e.g. for the modification of nanoobjects, an alternative experimental design still needs to be adapted. In order to circumvent the problems mentioned above, BPE in a capillary electrophoresis set-up can be carried out (51). The so-called Capillary-Assisted Bipolar ElectroDeposition (CABED) approach was the first attempt to use a capillary electrophoresis set-up for bipolar electrodeposition, exemplified by the site-selective modification of carbon nanotubes (52). The extremities of a capillary are placed into two compartments where the two feeder electrodes are located and are connected to a power supply. The capillary is filled with the electrolyte solution, containing the nanoobjects as well as the metal precursor, which needs to

be electrochemically reduced. With such a set-up, a potential difference of up to 30 kV can be applied, corresponding to electric fields of the order of 150 kV m^{-1}. In this way, parasitic reactions at the feeder electrodes are confined to the reservoirs and do not affect the bipolar process occurring inside the capillary.

Obviously, many other cell designs can be imagined, more or less related to - or being hybrid configurations of - the above-mentioned cases. Some of them are treated in more detail in the frame of the different specific applications discussed below.

3. Materials chemistry with BPE

Electrodeposition is a simple and efficient way to modulate the properties of a conducting surface. Therefore, BPE has been used to induce at least two different physico-chemical properties on either 2-dimensional or 3D conducting objects. Thus, this kind of modification leads in many cases to Janus particles (50, 53, 54). There are two ways to modify surfaces by BPE, which are direct and indirect electrodeposition, respectively. In the following section, we will present these two methods. Then, we will illustrate how BPE can be employed to study corrosion phenomena. Finally, this section will also describe bipolar electrodissolution as a readout system and as an original method to prepare material gradients.

3.1. Direct BPE electrodeposition

Among all electrochemical methods, direct bipolar electrodeposition is the main approach to produce asymmetric particles. The concept involves a solution containing the precursor species, which will exchange its electrons directly with the BE to generate a layer at its surface. Bradley and coll. reported the first Janus particles produced by BPE (28). They electrodeposited palladium on graphite particles. This was the beginning of direct bipolar electrodeposition using a metal precursor. Noble metals can be generated very easily due to their high standard potential, facilitating the electrochemical reduction of the corresponding precursors. In addition to palladium, gold ($E°(AuCl_4^-/Au)$ = 0.93 V/SHE) and platinum $E°(PtCl_4^{2-}/Pt)$ = 0.76 V/SHE) have been tested as well in this context (55). Naturally, other less-noble or non-noble metals can also be deposited, such as silver, copper, nickel, and zinc. These materials have been deposited at different scales, from millimeter-sized objects down to nanoparticles (Figure 2) (50),(52),(56),(57),(58). The size of the BE is an important parameter as it will significantly affect the value of the electric field that needs to be applied. As explained above, the smaller the BE, the higher is the intensity of the required electric field. The counter-reaction that occurs during the reduction of these metal salts is often water oxidation. However, even for depositing noble metals, applying the necessary high electric field is not trivial. In conventional configurations, the heating of the solution and the strong gas evolution can significantly disturb the bipolar electrochemical reaction. Kuhn and coll. solved this problem by using capillary electrophoresis (59) to carry out the bipolar reduction of gold salts on short carbon nanotubes (Figure 2c) (52). Normally, during the bipolar electrochemical reaction, only one side of the BE can reduce the metal ions present in the

solution. However, the BE can also be modified on both sides with the same metal as has been demonstrated with carbon microtubes modified with copper (60). Starting with an acetonitrile solution containing Cu^{+}, a first potential pulse was applied for 30 sec., to reduce copper cations into metallic copper. During this first step, all the tubes were aligned with respect to the electric field. Then, the tubes were allowed to move freely for 5 min. to adopt a random orientation, meaning that statistically half of the tubes change their orientation, prior to applying a second potential pulse. Repeating this sequence several times, leads to a symmetrical modification at both extremities of the BEs.

Due to the potential gradient generated along a BE, and because the deposition rate depends on the local polarization, a gradient in composition, thickness, morphology, color, and other physico-chemical parameters can be easily generated on BEs. Direct bipolar electrodeposition is a powerful tool to synthesize rapidly and in a straightforward way, material libraries. Among others, this allows to screen alloy properties. For example, an Ag-Au alloy gradient has been deposited on a stainless steel BE. The rate of electrodeposition of Au and Ag varies along the length of the BE, and consequently the chemical composition does also change as a function of the lateral position alongside the BE. This method allows e.g. identifying the best alloy composition to obtain an optimal surface-enhanced Raman scattering (SERS) intensity (61). Another example is the synthesis of a CdS gradient on a gold electrode. In this case, three distinct areas can be identified, one containing mostly S, another one with CdS, and the last part with a mixture of CdS and Cd, which can be identified by Raman and Auger electron spectroscopy (62). With the same philosophy, a Ni-Cu alloy gradient has been prepared in one step by BPE (Figure 2e) (63, 64), and it is even possible to co-electrodeposit up to three metals, Cu, Ni, and Zn on the cathodic side of a BE with a ratio that varies along the BE. The order in which the species are deposited corresponds to the respective standard potentials. Copper, which is the easiest to deposit, covers most of the cathodic part of the BE, followed by nickel and zinc, the latter being located just at the very extreme end of the BE (58). Gradients can be obtained on flat surfaces (65, 66), but also on cylindrical carbon fibers, allowing the screening of different deposit morphologies (67).

A gradient in size and spatial distribution of gold nanoparticles was reported by Lundgren *et al.* By addressing a BE, initially covered with a homogenous layer of gold nanoparticles, in a $HAuCl_4$ solution, they followed the modification during the BP electrochemical experiment. They observed an increase of particle size on the cathodic part of the BE (68). Li *et al.* also observed a gradient in the size of nanoparticles, directly electrodeposited by BPE. However, in this case, silver nanoparticles were generated on TiO_2 nanotubes. They studied the antibacterial activity of these nanoparticles as a function of their size (69).

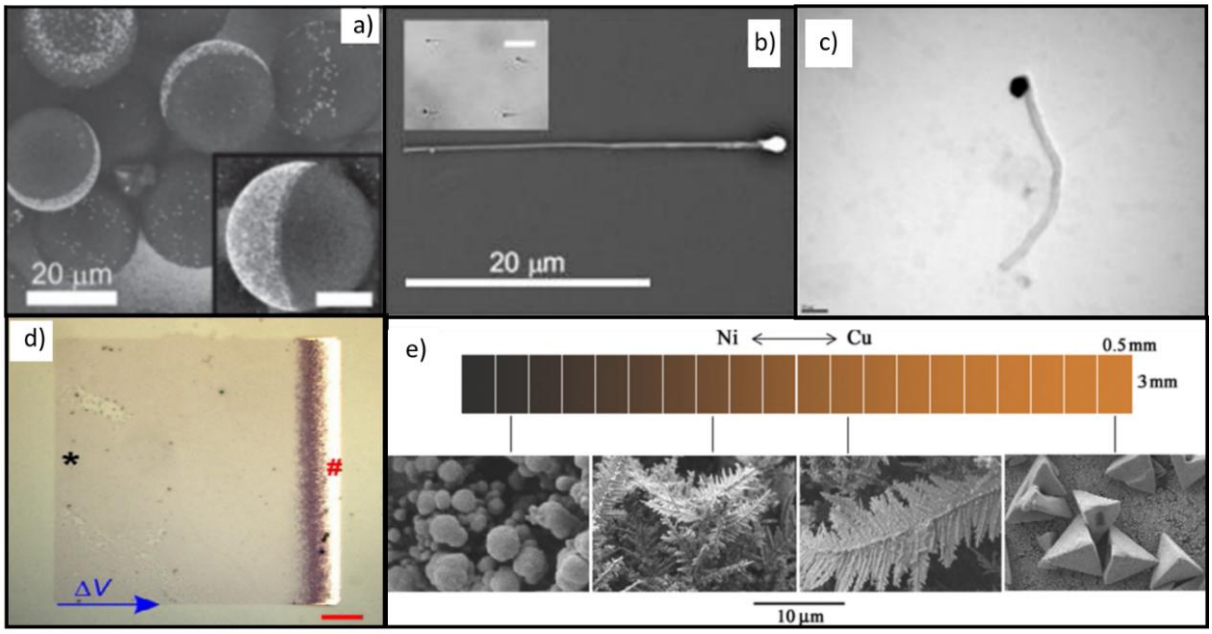

Figure 2. a) Scanning electron microscope (SEM) pictures of glassy carbon Janus beads with different diameters (20-50 µm) modified by gold (50), reproduced with permission from Wiley-VCH). b) Nickel deposit on a carbon microtube. Inset: optical image of several modified carbon microtubes (60), reproduced with permission from Elsevier). c) Transmission electron microscope (TEM) picture of a carbon nanotube modified with a gold cluster, scale bar: 50 nm (reproduced with permission from ref. (52). d) Optical image of a rectangular single graphene sheet (80×70 µm^2) modified with copper (right side), scale bar: 10 µm (from ref. (70), reproduced with permission from Wiley-VCH). e) One-step deposition of Ni_xCu_{1-x} alloys by BPE with a dual composition and morphology gradient (from ref. (63), reproduced with permission from Elsevier).

By electrodepositing Au through a closed-packed monolayer of uniform latex nanospheres, Kayran *et al*. obtained gold nanovoids after dissolution of the latex nanospheres. The thickness and roughness of these nanovoids vary with the potential gradient along the BE. They used this method to determine the experimental conditions that will result in optimal nanovoids allowing the emission of the most intense SERS signal after the adsorption of 4-nitrothiophenol (71). In another example, a simple gradient of copper, electrodeposited by BPE, results in three zones with distinct morphology, a dendritic shape at the edge, followed by a less dense dendritic area, and an area where only irregular nanostructures are visible. By modifying the surface with 1-dodecanthiol, the edge of the BE became hydrophobic, whereas the middle showed a more hydrophilic character. This modification allows water droplets to move spontaneously on the surface, from the hydrophobic to the hydrophilic area. This experiment illustrates the possibility of tailoring superhydrophobic surfaces (72).

BPE can control not only the shape but also the orientation of the deposit. Using an original BPE cell comprising 4 feeder electrodes, Fattah *et al.* managed to control the local deposition of copper particles on carbon microtubes by changing the direction of the electric field. A

first electric field, which is strong enough to orientate the microtubes, but not sufficient to trigger BPE, was used. Dimethyl sulfoxide was employed as a solvent, because its high viscosity at low temperatures allows freezing the spatial orientation of the BEs before starting the bipolar electrochemical reaction. Different types of deposits were obtained, one in alignment with the axis of the microtube, and another one at an angle of 90° (57).

The control of the local deposition by BPE is sufficiently precise to enable even the preparation of barcode type structures. Metallic rings could be electrodeposited on spherical BEs. The formation of these rings can be obtained by selecting anionic precursors (such as $AuCl_4^-$) that migrate towards the feeder anode. Therefore, on their way they first travel alongside the positively polarized portion of the BE where no electrodeposition is possible. While migrating along the surface of the BE, they finally encounter the frontier between the anodic and cathodic sides of the BE, where their reduction becomes possible as a result of an interplay between migration, diffusion, and electron transfer (73). In contrast, when a cation is employed as precursor, no rings are generated, but classic Janus particles are obtained.

BPE can also be employed to write a specific pattern on a surface. Braun *et al.* developed the Scanning Bipolar Cell (SBC). The SBC is composed of a microjet nozzle that allows depositing the electrolyte locally with the help of a pump. The anode is inserted inside the stream and the cathode at the end of the nozzle. Applying a potential difference between the two electrodes polarizes the surface which is in contact with the electrolyte, and thus it was possible to locally electrodeposit copper and gold (74),(75),(76).

Direct bipolar electrodeposition had also been used to establish electrical contacts between two copper particles. Putting the copper particles inside an electric field, one part of a given copper particle is dissolved by oxidation. Simultaneously, a reduction reaction occurs on a neighbouring second particle, allowing the directional growth of a copper wire between these two particles (29). This method has been used to generate electrical contacts on a commercial electronic circuit board (77). Using the same methodology, Sanjuan-Alberte *et al.* have reported the growth of silver microwires on silver particles for bioelectronic interfaces (78).

In order to generate well-defined nanorods, Koizumi *et al.* employed a porous anodic aluminium oxide membrane deposited on a gold electrode as a template. The ions migrate inside the nanoporous electrode by an electrophoretic effect induced by the electric field. They synthesized robust Co and Pt nanorods, as well as polymer nanowires (79),(80).

Most of the time, the chemical nature of the BE is either metallic or a carbon allotrope. However, semiconductors can also be used as BE, such as $MoSe_2$,(81) organic crystals,(82) or TiO_2 (82). TiO_2 is one of the most popular materials to produce hydrogen from water by using light energy. It is stable, low cost, but one of its drawbacks is that it absorbs mainly in the UV and that the charges recombine before they can react, resulting in low efficiency. To overcome this problem, it is possible to combine it with a noble metal that will induce a better charge separation and shift absorption of light in the visible (83). BPE is a promising technique to generate metal deposits on semiconductors such as TiO_2. n-type TiO_2 nanofibers have been modified by BPE under illumination. When the nanofibers are dispersed in a gold

salt solution, they get covered randomly with gold deposits during illumination. However, in the presence of an additional electric field, electrons and holes are directed towards opposite extremities of the fibers. Finally, a gold deposit is obtained exclusively at one end of the BE (84). The combination of light and electric field makes the modification of semiconducting BEs even easier compared to conducting BEs of the same size, because the main driving force is no longer the electric field but the illumination. Tiewcharoen *et al.* modified anatase TiO_2 nanoparticles with this method. An electric field with an amplitude of 3 MV/m is usually required to deposit gold on a conducting BE with a characteristic size of 100 nm. However, under UV illumination, deposition of gold was observed even when applying only 3 kV/m, meaning a gain of three orders of magnitude. This can be explained by the fact that an internal electric field is established inside the particle, which separates the holes and the electrons and the energy for the bipolar reaction is provided by the bandgap of the semiconductor. With this method, gold deposition occurs at the positive side of the BE and not at the negative side (85, 86).

Another way to avoid applying a high electric field for generating Janus objects is to use a closed configuration. Ongaro *et al.* deposited TiO_2 and CuO_2 semiconductors on gold nanowires, initially trapped inside a membrane. By using this closed configuration instead of the open configuration, all the current has to go through the BEs, and therefore a low potential is enough to achieve such a modification (87).

In order to diversify the applications of the particles produced by BPE, the electrodeposition of organic layers has also been studied. First of all, conductive polymers were deposited by BPE. Conductive polymers, produced by oxidation of monomers, such as polypyrrole and polythiophene, can be deposited simultaneously with a metallic layer. While the conductive polymer is formed at the anodic part of the BE, the metal can be deposited at the cathodic part. The deposition of the metal layer under these conditions requires a lower electric field compared to the one used in the absence of monomer, because its oxidation occurs at a lower potential than that of the solvent. Carbon microtubes with one side modified by copper and the other side modified by polypyrrole, as well as carbon microfibers modified with gold and polythiophene were prepared (55),(60). BPE can also be employed to generate conducting polymer microfiber networks (88). The electropolymerization of pyrrole had also been carried out in an ionic liquid. Usually, BPE is mainly performed in electrolytes with low conductivity. However, Kong *et al.* demonstrated that polypyrrole can be generated by BPE with 1-butyl-3-methylimidazolium bis(trifluoromethylsulfonyl)imide, [BMIM][TFSI] as an electrolyte, despite its relatively high conductivity of 4 mS cm^{-1}. This opportunity is interesting because ionic liquids have some advantages, such as low volatility, low flammability, and a large electrochemical window (89). Also, the polypyrrole film obtained under these conditions was more homogenous and smoother than the one synthesized in acetonitrile having an equivalent conductivity (90).

The reduction of diazonium salts is also an original way to obtain organic layers at the surface of a BE. When a carbon BE is used, covalent bonding is established between the organic layer and its surface. This anchoring layer makes it possible to bind also subsequently other molecules to the BE (91),(92). Koefoed *et al.* used BPE to achieve simultaneous anodic

and cathodic modifications, starting with only a single precursor molecule, 4-aminoethyl-benzenediazonium. This molecule features a diazonium moiety that can be reduced and an amino moiety that can be oxidized to form a C-N bond with the surface. Consequently, both sides can be modified in a single step (93). Iodonium and sulfonium salts have also been electrografted. Bands of grafted molecules were obtained at variable positions by tuning the applied potential (94). Graphene, deposited on insulating surfaces, has equally been functionalized by an organic layer based on the local electroreduction of 4-bromobenzenediazonium (95). Using an aqueous and an immiscible organic solution, two different molecules can be simultaneously electrodeposited on a BE positioned at the liquid/liquid interface with the advantage that the two grafting agents can not react with each other because they are dissolved in two different phases (96). With a configuration close to the one proposed by Braun and Schwartz (74), Zhou *et al.* combined an insulating cylinder with stainless steel feeder electrodes. The two feeder electrodes have a spiral shape and are positioned one above the other. By placing the cylinder with the feeder electrode above a conductive surface, electropolymerization of 3,4-ethylenedioxythiophene (EDOT) has been achieved. Local polarization allows patterning the surface with the polymer, triggering eventually the growth of perpendicularly orientated PEDOT fibers (97).

3.2. Indirect BPE electrodeposition

Indirect bipolar electrodeposition can be employed to generate deposits from non-electroactive precursors. In this case, water electrolysis is often used to trigger the electrodeposition of materials on the surface of the BE, due to a pH decrease on the anodic side and an increase in pH on the cathodic side of the BE. Loget *et al.* reported the local formation of TiO_2 and SiO_2 by polycondensation based on this method. Indeed, the sol-gel process starts with the polycondensation of monomers, resulting in a colloidal solution (sol) that acts as a precursor for the generation of an integrated network (gel). Tetraethyl orthosilicate (TEOS) has been used to generate a deposit due to the local pH increase at the cathodic side of a BE. Titanate could be deposited by using the opposite reaction at the anodic side, leading to a decrease of pH (98). The same principle also allows to deposit an electrophoretic paint on the anodic side of carbon fibers and on vertically aligned carbon nanotube arrays trapped inside an anodic aluminium oxide membrane. The paint is initially soluble in its basic form, but when the pH decreases, the carboxylate groups of the paint get protonated, causing its precipitation on the anodic pole of the BE. The deposition of the paint has been combined with the indirect electrodeposition of a thermoresponsive polymer, poly(N-isopropylacrylamide) (pNIPAM), to develop a system able to store and deliver molecules. In order to achieve the formation of the pNIPAM, the initial solution contains the monomer NIPAM, and an initiator, potassium persulfate. The reduction of the persulfate generates a radical anion that initiates the polymerization. In a single step, a nanoporous reservoir can be generated, because on one side the thermoresponsive membrane allows the uptake and delivery of molecules, while the opposite side remains closed by the electrophoretic paint (Figure 3a) (99).

The same type of electrophoretic paint has also been used to modify zinc particles in an asymmetric way in order to generate microswimmers. By applying the electric field, one

extremity of the zinc object is oxidized. The locally generated Zn^{2+} cations react with the carboxylate groups of the paint, triggering its precipitation. When the resulting asymmetric object is transferred in an acidic solution, H_2 bubbles are produced only on the side without paint, leading to a propulsion of the particle in a preferential direction (100). Based on an analogue philosophy, metal-organic frameworks (MOFs) have been generated at the anodic side of a BE. Starting with a zinc BE, Zn^{2+} is generated by the local oxidation of the BE. These ions react with 2-methylimidazole (2-MeIm), initially present in the solution, to form a Zn-imidazolate network [Zn(2-MeIm)$_2$], ZIF-8. Using the same principle, but with copper beads, HKUST-1 with the chemical formula [$Cu_3(BTC)_2(H_2O)_3$] (BTC=1,3,5-benzentricarboxylate) has been prepared based on the formation of Cu^{2+} by the direct oxidation of the copper bead and its reaction with 1,3,5-benzenetricarboxylic acid (Figure 3b) (101).

The Huisgen click reaction is a Cu^+ catalyzed 1,3-dipolar cycloaddition of an alkyne and an azide to form a 1,2,3-triazole (102). By using the local reduction of Cu^{2+} to Cu^+, Shida *et al.* triggered the click reaction on a conducting polymer (PEDOT) surface, functionalized with azide groups, in the presence of molecules terminated by an alkyne function. A gradient of Cu^+ is generated on the BE, leading to a molecular gradient of perfluoroalkyl groups immobilized on the polymer layer. By inverting the polarity, the authors were able to immobilize an alcohol group using the same procedure. The fluoro group being hydrophobic, and the alcohol group being hydrophilic, the authors measured a gradual variation of the contact angle when putting a water droplet on the polymer film (103). Silver objects can also be used for indirect BPE. Loget *et al.* oxidized silver nanotubes in order to generate silver chloride by indirect bipolar electrodeposition. The oxidation of silver generates Ag^+, which in the presence of Cl^- precipitates, leading to the localized formation of insoluble AgCl (50).

Ino *et al.* studied the electrodeposition of a calcium-alginate hydrogel by indirect BPE. In an electrolyte solution, containing sodium alginate and $CaCO_3$ particles, the oxidation of water produces H^+ at the anodic pole, resulting in the release of Ca^{2+} from the $CaCO_3$ particles. This local concentration of Ca^{2+} induces the deposition of a Ca-alginate hydrogel on an array of BEs. The authors successfully trapped living mammalian cells in the gel matrix, opening the way for the development of cell culture platforms (104).

Prussian Blue, which can be employed as a catalyst, pigment or in analytical chemistry, has also been electrodeposited by this indirect method. Starting with a solution containing ferric (Fe^{3+}) and ferricyanide ions ($[Fe^{+III}(CN)_6]^{3-}$), the local reduction of Fe^{3+} generates Fe^{2+} that reacts chemically with $[Fe^{+III}(CN)_6]^{3-}$, to form Prussian blue. The latter can be used for example to detect H_2O_2 in the presence of luminol by generating a chemiluminescent signal (105).

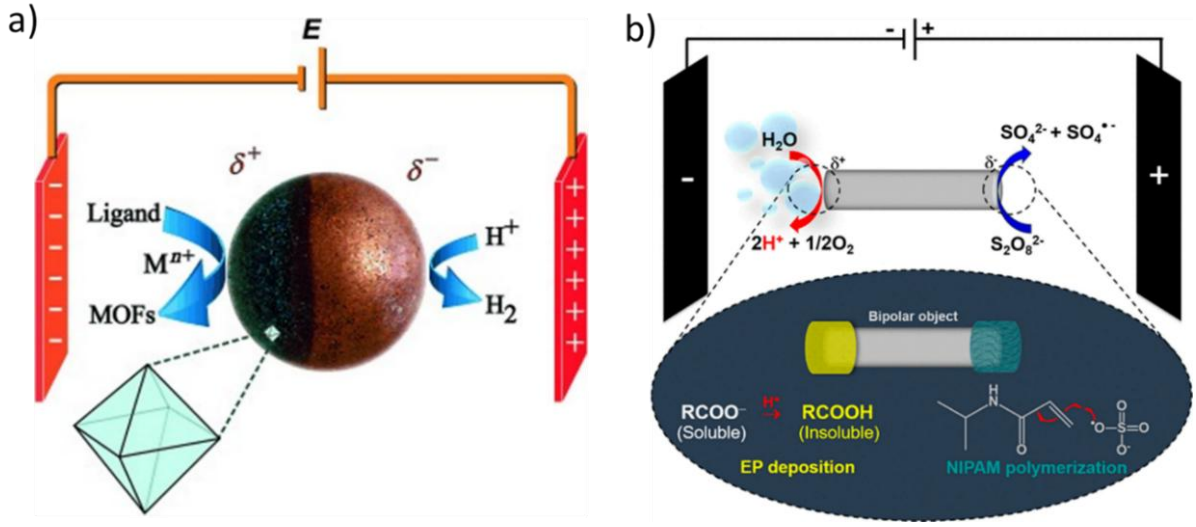

Figure 3. Scheme representing examples of indirect bipolar electrodeposition. a) Formation of a copper-based MOF (Adapted from ref. (101) with permission from Wiley-VCH). b) Precipitation of electrophoretic paint on the anodic side, and electropolymerization of NIPAM on the cathodic side of a carbon nanotube array (reproduced from ref. (99) with permission from the American Chemical Society).

Shida *et al.* prepared a gradient of polyelectrolyte brushes by BPE. This polyelectrolyte was prepared by the combination of BPE and electrochemically mediated atom transfer radical polymerization (ATRP) (106). A glass surface covered with the tethered initiator of the ATRP reaction is placed at a distance of around 100 μm above the BE. The BE reduces Cu^{2+} to generate Cu^{+}, which will catalyse the polymerization reaction on the surface of the glass plate. As the concentration of Cu^{+} varies along the BE, the polymerization will also take place with variable intensity on the initiator functionalized glass plate. Following this strategy, a gradient of poly-tert-butyl methacrylate has been generated. This initial layer can then be used to deposit layer-by-layer poly(diallyldimethylammonium chloride) and poly(sodium 4-styrenesulfonate) (107),(108).

3.3. Dissolution and corrosion

The potential gradient generated during the BPE experiment can also be used to learn more about corrosion processes, because a material can be oxidized simultaneously at different potentials in just one single experiment (109),(110). Björefors and coll. studied the corrosion of stainless steel with this technique. The advantage of this approach is the possibility to compare the behaviour of multiple samples in a single corrosion experiment. It is also possible to collect valuable information about the involved oxidation and reduction processes by just analysing one BE (13),(111). The corrosion of commercial stainless steel grade 2205 has been investigated in this way. Crevice corrosion, pitting corrosion, general corrosion, and a passivation region have been observed on the same electrode. A Luggin capillary was used to locally measure the potential above the BE in order to correlate the potential with the degradation of the different regions (14). On type 420 ferritic stainless steel, pit nucleation,

growth and coalescence were observed. Apparently, the pit growth kinetics is independent of the applied potential. With this method, it was possible to determine a critical pit volume for which the pit switches from metastable to stable. On a 50 mm long BE, after applying the electric field for 30 min, four distinct regions can be observed (Figure 4a). From the cathodic region to the edge of the anodic region, where pitting corrosion surrounded by general corrosion is present, a 3D image of these regions has been recorded (Figure 4b).

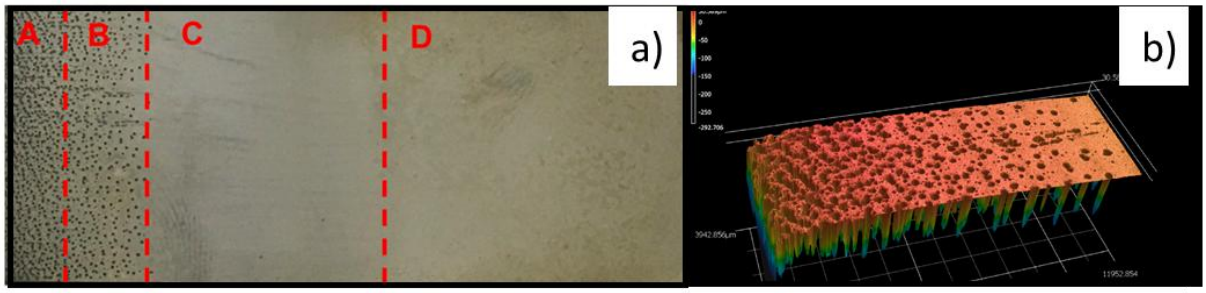

Figure 4. a) Optical image of a 50 mm-long BE (type 420 ferritic stainless steel) after 30 min of exposure to the electric field. Zone A: pitting with general corrosion, zone B: pitting, zone C: general corrosion, zone D: cathode. b) 3D confocal laser scanning microscope image of the pitting corrosion region (from ref. (112), reproduced with permission from mdpi).

BPE has also been employed to oxidize metals and generate metal oxides, such as aluminium oxide, Cu_2O (113), ZnO (114) and TiO_2, in open and closed configurations, with either DC or AC electric fields. Xu *et al.* used closed BPE to generate ordered porous alumina films by oxidation of an aluminium foil. Such films are popular as templates to prepare nanowires or nanotubes. The closed configuration improves the current density, leading to faster growth of the porous structure compared to a classic set-up (115). Self-organized TiO_2 nanotubes are interesting materials, for example as anodes in photoelectrochemical cells for water splitting (116), dye-sensitized solar cells (117) and biomedical applications (118). These nanotubes can be prepared by anodization of a titanium foil in the presence of fluoride anions (119). This approach allows a fine-tuning of their diameter and their length, as these features strongly depend on the applied potential. As already explained, BPE is a well-suited method to screen the effect of different potentials rapidly and in a straightforward way. Loget et *al.* used this method to prepare TiO_2 nanotubes with different diameters and lengths on the same titanium foil. On a single titanium foil, they obtained a ratio of 100 between the shortest and longest nanotubes. Furthermore, a ratio of 4 between the thinnest and the thickest nanotubes could be achieved. Studying their photoactivity locally with a laser allows a fast screening of the properties of the nanotubes in order to determine the best nanotube geometry leading to the highest photocurrent (120). Furthermore, it has been possible to decorate the nanotubes with Pt nanoparticles. A gradient of nanotubes in one direction has been combined with a gradient of Pt nanoparticles in the other direction, and the performance of the final hybrid nanotubes has been evaluated by mapping the local production of H_2 (121). A similar method was used by Saqib *et al.* to prepare multiple titanium foils with TiO_2 nanotube arrays. Using a thin layer of supporting electrolyte, it was possible to control the growth of the tubes in the horizontal direction instead of the classical vertical direction (122). A gradient of TiO_2

nanotubes has also been used to study the effect of the size and the crystalline phase on the behaviour of biological cells (123). A better adsorption of proteins is observed when the diameter of the nanotubes increases, while with thinner nanotubes the cell adhesion, proliferation and differentiation were better.

TiO_2 nanotubes have also been synthesized on Ti spheres by BPE. First, the beads (diameter of 3 mm) were immobilized between the two feeder electrodes on an adhesive tape. Using a square wave potential (±120 V), switching every minute for 200 min., the entire surface area of the sphere could be modified with longer tubes at the extremities of the sphere, whereas the length of the nanotubes was shorter at the center. The final TiO_2 nanotubes show a twice better photocatalytic activity for the degradation of methylene blue, compared to a normal titanium sphere (124).

Instead of performing BPE on a static object, it is also possible to introduce the BEs in a stirred compartment, separated from the electrode feeders. In this set-up, the BEs move randomly without touching the feeder electrodes, and consequently the electrochemical reactions take place uniformly on the surface of the BEs. This method was applied to copper beads with a variety of initial diameters. The beads were gradually oxidized, allowing to reduce their size in a homogenous way. Once the reaction is no longer possible, because the size of the BE becomes too small to allow a sufficient polarization, the process stops automatically. This wireless electro-induced milling results in beads of identical size (125).

The controlled electrodissolution of a metal film also provides a way to report a reaction occurring at the cathodic side of BEs. Crooks and coworkers employed this method to monitor hybridization events. They observed the oxidation of silver at the anodic section of the BE, which became only possible after the hybridization at the cathodic side. The loss of silver can be observed with naked eyes (126). This method has also been adapted to screen the performance of electrocatalysts used in the oxygen reduction reaction (ORR) (127), or to measure the concentration of nitrate ions (128). In the latter case, the length of the dissolution of the silver layer is proportional to the concentration of nitrate ions. On the other hand, oxygen evolution reaction (OER) was studied on a nickel (oxy)hydroxide gradient. A gradient of nickel was first electrodeposited on a fluorine-doped tin oxide (FTO) electrode. The substrate was then cycled in a basic solution in a three-electrode cell, with the modified FTO serving as working electrode. After converting the nickel gradient into the corresponding nickel oxide, the surface has been locally investigated with scanning electrochemical cell microscopy. The tip was a 10 µm pipet filled with NaOH solution (pH 12), 50 mM NaCl and a Ag/AgCl wire has been used as a quasi-reference electrode. A local electrochemical cell is formed when the tip is close to the substrate. Cyclic voltammetry measurements were performed to observe the OER along the nickel (oxy)hydroxide gradient. The measurement revealed large variations in the local catalytic activity along the gradient (129).

BPE can also be used to depollute water. Electrocoagulation is a powerful method to treat wastewater (130). The oxidation occurring at an anode generates metal cations that can form metal hydroxide particles via a reaction with the hydroxyl ions generated during the water

reduction at the cathode. The resulting particles can form aggregates with the pollutants present in the aqueous phase. Qi *et al.* used BPE to dissolve the anodic part of a BE, leading to the formation of positively charged ions, such as Fe^{2+}or Fe^{3+} in the case of a sacrificial anode made out of iron, and Al^{3+} if aluminium is used. Then these cations react with the hydroxyl ions generated at the cathodic part of the BEs. Due to the intrinsic features of BPE, it is possible to work without a physical connection to the electrodes, thus allowing a large number of electrodes to be used simultaneously for a more efficient depollution (131, 132).

The electrochemical exfoliation of graphite has been of great interest due to produce graphene and graphene oxide. For the mass production of graphene oxide, anodic exfoliation is an extremely attractive concept (133). In this context, a bipolar electrochemical exfoliation concept has been developed by Hashimoto *et al.* After identifying the best experimental parameters, such as electrolyte concentration and electric field strength, with a large graphite plate, the method has been applied to graphite powder, in order to obtain a large number of graphene oxide nanosheets (134). Black phosphorus is another example of two-dimensional materials that can be obtained by exfoliation. Baboukani *et al.* used BPE to produce black phosphorus nanosheets (called phosphorene) from the initial bulk material. The H^+ and HO^- ions generated at each extremity of the BE during water electrolysis can be intercalated into the black phosphorus, resulting in phosphorene particles. These particles are automatically deposited on the positive feeder electrode due to electrophoresis effects occurring in the cell. A modified surface can be generated in a single step by exfoliation of phosphorus material, and the resulting electrode has been tested successfully for capacitive energy storage applications (135).

4. BPE for motion generation

The development of mobile actuators is still an emerging hot topic that has attracted a massive interest over the past decades (136-141). In order to explain such a strong scientific emulation, one has to consider that these mobile systems are as interesting from a fundamental point-of-view, than for potential applications such as purification and treatment of contaminated solutions or forefront clinical diagnostics or surgery (142-144). In fact, this field of research gathers two distinct communities. The first one includes solid-state chemists who design particles that can propel themselves when dipped inside a solution containing a given chemical fuel. The second one is composed of physico-chemists that employ physical forces such as magnetic or electric fields in order to generate and control motion. Both approaches are rather complementary, but the key common feature is the necessity to break symmetry in a 3-dimensional space. In this sub-section, for reason of clarity, we will focus on the fundamental mechanistic aspects without discussing in details the potential applications.

4.1 Self-powered motion

A very widespread strategy to propel swimmers in solution involves the use of a chemical fuel (136). This is indeed a rather simple idea, since the process is intrinsically based on

redox chemistry. However, a key point remains the necessity to use an asymmetric object, because the redox reactions should take place in an anisotropic way. In that context, the two main mechanisms of motion involve an action/reaction principle that can be explained either by the generation of gas bubbles or by self-electrophoresis. In fact, these two propulsion mechanisms depend very much on the size of the object. Practically, bubble-based propulsion is mainly responsible for the motion of macroscale objects, whereas self-electrophoresis seems to dominate at the micro- and nanoscale. Self-electrophoresis explains the propulsion of bimetallic nanorods immersed in a solution containing H_2O_2 fuel (Figure 5a) (145, 146). These asymmetric nanorods are fabricated by electroplating and/or processes adapted from soft lithography techniques. Typically, they are composed of two segments made out of different metals and can be considered as intrinsic BEs, featuring two poles where H_2O_2 is oxidized or reduced, respectively. At the same time, a proton gradient is established with H^+ moving from the local anode towards the cathode, thus inducing electrokinetic motion. The initial work in this field reported the use of a bimetallic nanorod with Pt and Au segments (147, 148). This first generation of swimmers was 2-µm long and reached typically a speed of up to 4 body lengths per second when exposed to H_2O_2. A large number of different metal compositions were tested including Ni, Ru, Rh, Pd, Pt, and Au, to investigate in detail the propulsion mechanism (145, 146). Also, a comparison was made with a segmented nanorod in which the gold moiety is combined with a polypyrrole end containing catalase. This enzyme decomposes H_2O_2 according to a biochemical mechanism and it was found that the catalytic reaction occurred at a comparable rate to that of electrochemical bimetallic segments.

The optimisation of the fabrication method enabled processing more complex combinations featuring multiple metal segments. In this context, the authors used a trimetallic nanorod with up to five consecutive segments, two out of five containing nickel, in order to complement the bipolar propulsion with magnetic guiding capability (149). Several strategies have been proposed to reach higher speed, such as the use of carbon nanotubes to increase surface roughening, resulting in a substantial acceleration with a speed limit of up to 100 µm per second (150). However, the ground-breaking strategy was to move from rods that were completely filled with metal to tubular pipes (151-155). Several template based approaches were proposed, but a classic example is illustrated in Figure 5b. The idea is to electrocatalytically generate bubbles that will be collected, directed and released across the tubular shape. Such a strategy enables a much higher speed limit of up to 2,000 µm per second in the case of a layered structure comprising three metals, in which a sacrificial silver layer is employed to generate the void part inside the microjet.(153). This new propulsion mode was quantitatively compared to the former self-electrophoresis propulsion and the corresponding energy conversion efficiency was found to be one order of magnitude higher.(156)

Another key step towards the design of new swimmers was proposed by translating the propulsion into a rotational motion.(157) For that, a Pt/Au bimetallic nanorod was post-modified, so that one side of the 5-µm rod was decorated with an Au/Cr bilayer, providing

the essential break of symmetry. Therefore, only half of the Pt segment was exposed to the chemical fuel, resulting in an anisotropic driving force. The length ratio between Pt and Au segments was found to be the key parameter to control the rotation speed with an optimum ratio of two (*i.e.* the Pt segment is twice longer than Au segment) leading to a limit of almost 25 rpm. It is noteworthy that the same kind of approach was proposed to elaborate autonomous Pt-based rotors by means of bipolar electrodeposition (158). Again, the break of symmetry remains the central ingredient since an isotropically positioned Pt cluster induced a linear propulsion, whereas an asymmetric deposition enabled a rotation instead. A comparable rotation speed of 30 rpm was monitored with a 20 µm-long carbon microtube featuring an off-centred Pt cluster at one extremity.

Apart from H_2O_2, which is the most frequent chemical fuel that is used to propel microscale swimmers, several other reactants have already been proposed. For example, Mallouk, Sen and co-workers generalised the concept of self-propelled swimmers to another fuel than hydrogen peroxide by using hydrazine (159). Furthermore, it is possible to control the direction of locomotion by selecting the proper fuel. This was demonstrated by comparing the propulsion of a Pd/Au bimetallic nanorod with hydrazine and dimethylhydrazine, respectively. The reason is due to a shift in the measured mixed potential in both solutions, which in turn reverses the intrinsic polarity of the two segments with respect to the bipolar reactions. The use of aqueous bromine and iodine solutions was also studied (160). The proof-of-principle was reported by using Pt/Cu bimetallic nanorods and, as before, the propulsion mechanism involves self-electrophoresis. Interestingly, the electrochemical reactions differ slightly between Br_2 and I_2 solutions. In the first case, HBrO is reduced to Br^- at the Pt pole in combination with copper dissolution to form Cu^{2+}, whereas I_2 reduction is coupled with CuI formation in the second case. It is noteworthy that other electrocatalytically active metals were also proposed such as zinc or magnesium that promote hydrogen evolution in acidic aqueous solutions (100, 161-163). In some cases, the corresponding swimmers were synthesized by BPE with a break of symmetry provided through the local deposition of an electrophoretic paint. A zinc/polymer dendrite was used as a proof-of-principle whereas the case of magnesium was studied in more depth to demonstrate the influence of the degree of asymmetry on the tortuosity of the trajectory.

4.2 Externally driven motion

In contrast to the previous case, externally driven motion is based on the application of an external field in order to promote the movement of a given object. One possibility is obviously to employ a magnetic field to control the position and/or the motion of a magnetic actuator, however this situation will not be developed in this chapter. Also, the case of an external electric field will be only discussed in the frame of BPE, meaning that neither electrophoretic nor electroosmotic motion will be presented in this sub-section. The main mechanism of motion that is considered here relies on the direct application of an electric field to address a BE where the involved electrochemical reactions will lead to a well-defined motion. This general concept has been initially reported in the 2010s (164, 165).

Horizontal motion was first described based on two different mechanisms. The first case corresponds to a bipolar metal electrode made out of a zinc dendrite that is positioned inside a capillary filled with an aqueous $ZnSO_4$ solution (164). The application of only a modest electric field is sufficient to overcome the overpotentials needed to promote the anodic dissolution of zinc together with Zn deposition on the cathodic pole. *In fine*, the dendrite translates continuously towards the feeder anode. From a conceptual point of view, one can argue whether the observed translocation can be considered as real motion, as the zinc dendrite continuously changes its shape and length during its movement. In fact, the phenomenon could be considered as the propagation of a chemical wave, driven by an electric field. In principle, such a strategy can be potentially applied to a variety of non-noble metal particles. An analogue concept was later used for the propulsion of a sacrificial copper BE in folded fluid channels (166).

On the other hand, an alternative approach was also proposed and involved the site-selective production of gas bubbles (Figure 5c). The evolution of hydrogen or oxygen can be used, but practically H_2 bubbles are more efficient due to the stoichiometric advantage of this reaction. The locomotion of carbon beads of several sizes could be achieved by applying an increasing driving force when downsizing the length of the BE. Vertical motion was also reported by fitting a simple conducting bead inside a capillary filled with an aqueous solution (167). The idea is to select the polarity of the feeder electrodes in order to develop a cathodic site at the bottom of the bead and therefore to generate H_2 gas below the object. The bubbles can readily accumulate and lift the bead in the direction of the feeder cathode that is positioned at the top of the capillary. Initially, the anodic reaction converted a sacrificial chemical species, but one can select advantageously another specific oxidation reaction to obtain an additional level of functionality. This was demonstrated with anodic electrogenerated chemiluminescence (also noted, electrochemiluminescence or ECL) that can be recorded *in situ* while the bead is moving inside the capillary (168). The proof-of-principle experiment was performed with $[Ru(bpy)_3]^{2+}$ (tris(2,2'-bipyridine)ruthenium) or luminol (3-aminophthalhydrazide) dyes with tri-*n*-propylamine (TPA) or H_2O_2 as co-reactants, respectively (168, 169). Interestingly, the direction of motion depends on the choice of chemicals that are involved in the electrochemical reactions. For Ru-based ECL, hydrogen evolution is responsible for the vertical motion, and red light ECL is observed on the opposite side. Typically, the bead is moving towards the feeder cathode (168). On the contrary, in the case of luminol-based ECL, O_2 bubbles are produced by oxidation of H_2O_2 accompanied by blue light ECL observed on the same side. In that case, the bead moves in direction of the feeder anode (169). Another possibility is to select an enzymatic system that produces *in situ* the ECL co-reactant. This was achieved with a glucose dehydrogenase by employing nicotinamide adenine dinucleotide (NAD^+) as a co-factor. The enzymatically-produced NADH is involved in $[Ru(bpy)_3]^{2+}$ ECL according to a classic reductive oxidation pathway. Also, the amplitude of the ECL signal is directly related to the local glucose concentration (170). The major limitation of this strategy is that the diameter of the bead that is used as BE should fit the size of the capillary (167). However, this limitation has been overcome by designing a second generation of BEs

featuring a set of conducting arms combined with a small reservoir enabling the collection and controlled release of the electrogenerated bubbles (171). This leads to an object that can be successfully actuated in a 2-dimensional space. Also, in this work the integration of a light-emitting diode (LED) into these swimmers was proposed to allow light emission during the motion. In this context, the very simple electrochemical addressing of a LED by wireless BPE is illustrated in Figure 5d. The LED has been immobilized at the bottom of the electrochemical cell and one can easily see the light emitted from the LED that is driven by water electrolysis.

Over the years, this rather fundamental research area was adapted for the design of more sophisticated devices. For example, a bipolar electrochemical valve was described as a true wireless actuator (172). Again, the electrochemical mechanism involved the stepwise production and release of H_2 bubbles. The rate of gas formation controls the alternating actuation of the valve. Several rotors were also engineered by assembling BEs thus enabling a rotational motion in either a vertical or a horizontal plane (165). The possibility to couple these motors with ECL has also been achieved with a second generation of rotors (173). In this case, the arms of the rotors were modified with reservoirs that can accumulate and release gas bubbles as a function of their orientation. Simultaneously, ECL was generated at the anodic arm, leading to a light-emitting device whose rotation can be tracked by ECL (Figure 5e).

More recently, a new generation of conducting polymer-based crawlers was also reported based on a triple symmetry breaking (174). For that, polypyrrole was selected since its redox state triggers either its swelling or shrinking, leading to a wireless deformation of the polymer film (175). Therefore, the latter can be used as a freestanding BE while the application of an alternating external voltage enables the stepwise motion of the crawler. The combination of this approach with an additional functionality such as light emission was exemplified by integrating a miniaturized LED inside the two polymers legs (176).

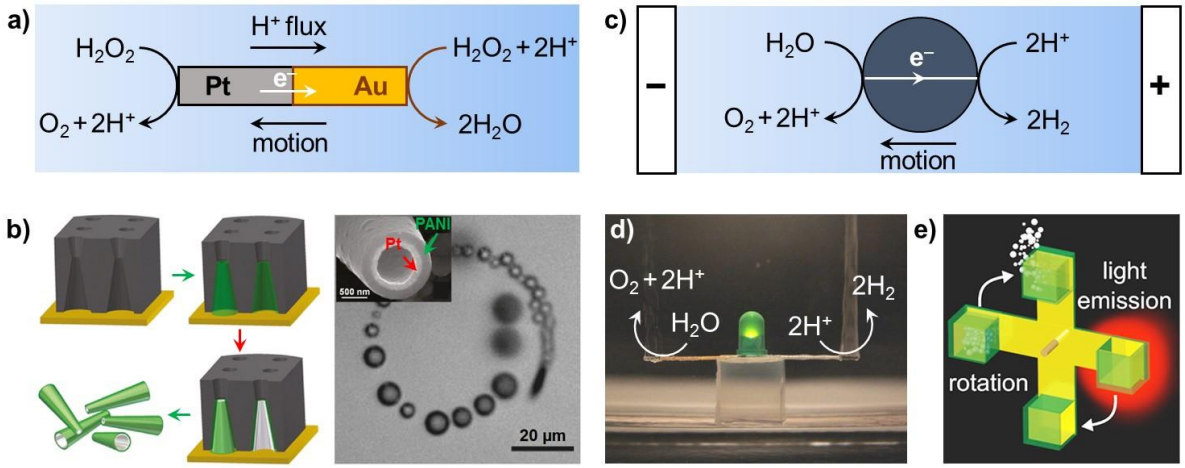

Figure 5. (a) Scheme of the propulsion mechanism of a bimetallic Pt/Au nanorod that can be considered as an intrinsic BE (adapted from ref. (146), reproduced with permission from

the American Chemical Society). (b) Scheme of the fabrication process of a polymer cone with an inner thin platinum layer and the corresponding mode of locomotion (adapted from ref. (155), reproduced with permission from the American Chemical Society). (c) Scheme of the bubble-induced motion of a spherical BE exposed to an electric field (adapted from ref. (165), reproduced with permission from Springer Nature). (d) Image showing the wireless actuation of a green LED. Water splitting is driven by BPE (adapted from ref. (171), reproduced with permission from Springer Nature). (e) Scheme of principle of a rotor whose motion is enabled by the stepwise production, collection and release of H_2 bubbles at the cathode pole. Simultaneously, red light ECL is generated at the anode by using $[Ru(bpy)_3]^{2+}$ luminophore (adapted from ref. (173), reproduced with permission from the American Chemical Society).

5. Bipolar (bio)electroanalysis

As illustrated in the two previous sections, BPE enables the synthesis of asymmetric particles and also the conception or actuation of mobile systems, leading thus to various applications. However, the most investigated field among all these possibilities remains the use of BEs for electroanalysis.

5.1 Sensing principles

At a first glance, employing BEs as platforms for sensing applications could be considered as counter-intuitive. This is especially true because of the technical difficulty to accurately measure the current that is flowing across a BE, since it is addressed in a wireless manner. In fact, this drawback can be easily circumvented because a BE offers many different experimental configurations and possibilities thanks to several key advantages in comparison to a classic electrode. As mentioned previously, there is no need for a physical connexion between the BE and the power supply. Also, the two most important parameters that govern the capability of a conducting object exposed to an electric field to behave as a BE are the size or length of the object and the strength of the applied electric field. Therefore, the position of the BE inside the electrochemical cell does not affect the corresponding interfacial polarization. Consequently, one single pair of feeder electrodes can be used to address simultaneously as many BEs as necessary. This offers the possibility to address very easily large arrays of patterned (micro)electrodes that are deposited or screen-printed on an insulating support. Another key feature of BPE directly relies on the fact that the bipolar object exhibits two electrochemical poles where the oxidation and reduction reactions take place simultaneously. Such a direct electrochemical coupling implies that the same amount of electrons produced at the anodic edge are transferred through the BE and are involved in the reduction process at the opposite side. In other words, there is strictly the same number of electrons involved in both electrochemical processes. Consequently, the archetypical strategy in analytical BPE is based on the use of one pole for the detection (i.e. sensing pole), whereas

the other one acts as a reporting pole. Again, as the measurement of the bipolar current is not trivial, the electrochemical reaction that occurs at the reporting pole is chosen in such a way that it can be easily visualized. In most cases, the sensing pole is the cathodic side so that a reduction reaction is detected. The reason is simply due to the fact that several anodic reactions offer a very simple visual signal that can be used as a readout. Therefore, the typical experimental configuration could be the following: a chemical species is dissolved in solution and gets electrochemically reduced at the cathodic pole of the BE when applying a sufficient electric field across the electrolyte. The same amount of electrons is involved in the oxidation process, leading to a fully correlated readout. By comparison, the same experiment conducted in the absence of the redox-active target will not generate any signal since the two electrochemical reactions cannot be coupled. In that case, no faradaic current flows across the BE, thus precluding the reporting signal.

The first reporting strategy was proposed in the early 2000s by two different groups and is based on ECL (177-179). The idea is to obtain an electrochemically-initiated light emission that is produced from a combination of reactants (generally a luminophore and a co-reactant) upon electrochemical oxidation. This is the most widely used analytical strategy and the vast majority of the publications in this field is based on this principle. Several mechanisms can be considered, but essentially the number of photons that are emitted is proportional to the number of electrons that are involved in the electrochemical process. In that case, the readout is directly the ECL signal that can be visualized either with the naked eyes for a simple On/Off sensor or monitored with a detector such as a charge-coupled device (CCD) camera or a photomultiplier tube (PMT) in order to quantify this output signal. Another popular reporting strategy was reported in 2010 by the group of Crooks and involved an anodic metal dissolution (126). According to this concept, either the cathodic pole or the entire BE is made out of a metal. An oxidation that occurs on the anodic side of the BE is coupled with the reduction on the other side and such a dissolution leads to a shortening of the BE. *In fine*, the kinetics of electrochemical processes can be compared since it affects the amplitude of the dissolution. Besides the two aforementioned strategies that are the most popular, other possibilities such as the use of a fluorescence signal, of an electrochromic layer or the electromechanical deformation of a BE have also been proposed (180-183). These examples will be developed in details in the next sub-sections.

5.2 Optical transduction

The intrinsic wireless nature of BPE implies that the electrochemical information, typically the faradaic current or the potential, cannot be measured as easily as in classic electrochemistry. This feature does not represent a significant problem for applications in material science or catalysis. However, the situation is different in the field of analytical chemistry, which requires the measurements of quantitative parameters. For a long period of time, it constituted a crucial practical impediment, limiting the development of analytical applications of BPE. To solve this issue, at least one of the redox reactions occurring at the BEs has to be associated with other techniques providing an optical readout. It means that the

electrochemical information has to be converted into an optical signal that is proportional to the faradaic current passing through the bipolar object. As detailed below, the transduction method may be based on easy observable optical signals produced by techniques such as colorimetry, fluorescence, electrochromism, light emission from LEDs, ECL or the anodic dissolution of metals. Briefly, ECL light emission occurs when the excited state of a luminophore is generated by a cascade of reactions, triggered by an initial electrochemical reaction at the electrode surface.

In the early 2000s, a seminal report from Manz and co-workers contained remarkable original ideas and suggestions on the possibility to combine BPE with optical detection, for high-throughput analysis and miniaturized analytical instruments (177). Indeed, in the same article, the authors demonstrated both colorimetric and ECL detection following electrophoretic separation as well as the coupling of imaging with BPE. In their simple experimental setup, a "U-shaped" Pt wire electrode was positioned across a separation channel (Figure 6a). The required electric field was imposed in the channel during electrophoretic separation. It polarized the "legs" of the "U-shaped" wire and triggered the corresponding bipolar reactions. They reported the colorimetric imaging of changes in the universal pH indicator colour around the BEs as well as around both feeder electrodes. Then, after the electrokinetic separation step, ECL emission was generated in this simple but very efficient bipolar configuration. ECL detection of two ruthenium-based luminophores and of three model amino acids was reported. However, in this approach, only the analytes involved in the ECL process, for example as the luminophore, the coreactant or a quencher may be detected directly. Crooks and co-workers proposed an alternative and powerful strategy to sense redox-active analytes, which are not directly involved in the ECL reaction (178, 179). They exploited the global electroneutrality conservation at the level of the BE, since it imposes that the oxidation and reduction currents are equal. In other words, the reduction current is intrinsically correlated to the oxidation one. Therefore, the electrochemical activity of the cathodic pole of the BE can be monitored by measuring an oxidation process, such as the anodic ECL emission. As a proof-of-principle, the authors reported the indirect detection of benzyl viologen in a microfluidic system (178, 179). They demonstrated that the ECL reporting reaction can be decoupled from the electrochemical sensing reaction (184). In a multichannel configuration, with a microelectrochemical bipolar device, the same group described the possibility to mimic some logic functions of solid-state circuit components such as diodes and transistors (185). DNA detection was achieved at a bipolar microarray sensor based on indirect ECL imaging (186). The bipolar gold electrode was functionalized with a 25-mer DNA capture probe using thiol chemistry (Figure 6b). Upon incubation with the target DNA labeled with 4 nm Pt nanoparticles, the capture of the complementary sequence was revealed by ECL emission at the anodic pole of the BE. In addition, three BEs were addressed simultaneously by BPE (186).

After these ground-breaking works, ECL became progressively the most popular readout strategy for BPE in the last two decades (5, 6, 32, 33, 37, 187). Indeed, by measuring the light intensity, ECL offers the possibility to observe indirectly the current flowing in the BE in a wireless manner. The development of bipolar ECL is mainly due to the complementarity of

both methods and to the notable advantages of ECL. Indeed, in appropriate conditions, the intensity of the ECL emission reflects the electrochemical activity (i.e. the faradaic current) of the BEs. In addition, ECL is a very sensitive analytical and imaging method, operating at physiological pH, with very low background signal, requiring only a simple experimental setup (just a photodetector such as a smartphone (168, 170, 188, 189) or a CCD camera (190) can be readily used). It can be easily combined with biomolecules such as enzymes, antibodies, nucleic acids, and cells. In the BPE field, the two most widely-used ECL couples operate in an oxidation regime and are $[Ru(bpy)_3]^{2+}$ luminophore (or its derivatives) with TPA as sacrificial coreactant, or luminol combined with hydrogen peroxide.

The analytical applications have been fuelled by the support of a theoretical framework for bipolar ECL (191-194). Crooks and co-workers demonstrated nicely the relationship between the faradaic current and the ECL intensity and their theoretical findings have been supported by experimental results (191). They showed that a threshold current must be reached before ECL is detected with a reporting sensitivity of ca. 7200 counts/nA in this experimental configuration (191). The length, the number and the shape of the BEs were investigated as well as the channel geometry (191, 195-198). An important point was also the demonstration of the ECL intensity as a function of the position along the BE. This original idea was further developed using "snapshot voltammetry" where a complete voltammogram may be extracted from a single ECL image recorded at the level of a triangular bipolar microelectrode (199). Indeed, the spatial distribution of the interfacial potential difference between solution and BPE governs the electrochemical driving force along the longitudinal axis of the BPE and, thus, the local ECL intensity. This overpotential gradient was mapped on a bipolar microelectrode array (200) and on BEs with various geometries (Figure 6c) with surface plasmon resonance imaging (SPRi) (201, 202). The control of a 2D electric field within four crossed microfluidic channels allowed manipulating the local potential difference with the solution and it was imaged by a map of the ECL emission (203).

Since BPE relies on controlling the potential of the solution, a single BE or several ones can be polarized remotely. Crooks and co-workers addressed 1000 individual BEs fabricated on an insulating surface by BPE (Figure 6d) (195). ECL imaging was employed to read the activities of all the BEs simultaneously. Since ECL is by essence a process confined to the immediate vicinity of the electrode surface, BPE opened the possibility to circumvent this limitation by generating ECL emission at the level of millions of micro/nano-emitters dispersed in solution (204). Every object (multi-walled carbon nanotube) is polarized by BPE and acts as an individual ECL emitter. Their collective behaviour enables strong ECL emission in the whole volume of the solution (204, 205). This approach has been further extended using a dispersion of carbon microbeads as bipolar elements for the imaging of two different analytes, choline and glucose, in an inhomogeneous sample (206). It was achieved using two enzymes, glucose dehydrogenase and choline oxidase, coupled with ECL systems emitting at different wavelengths, $[Ru(bpy)_3]^{2+}$/NADH and luminol/hydrogen peroxide, respectively.

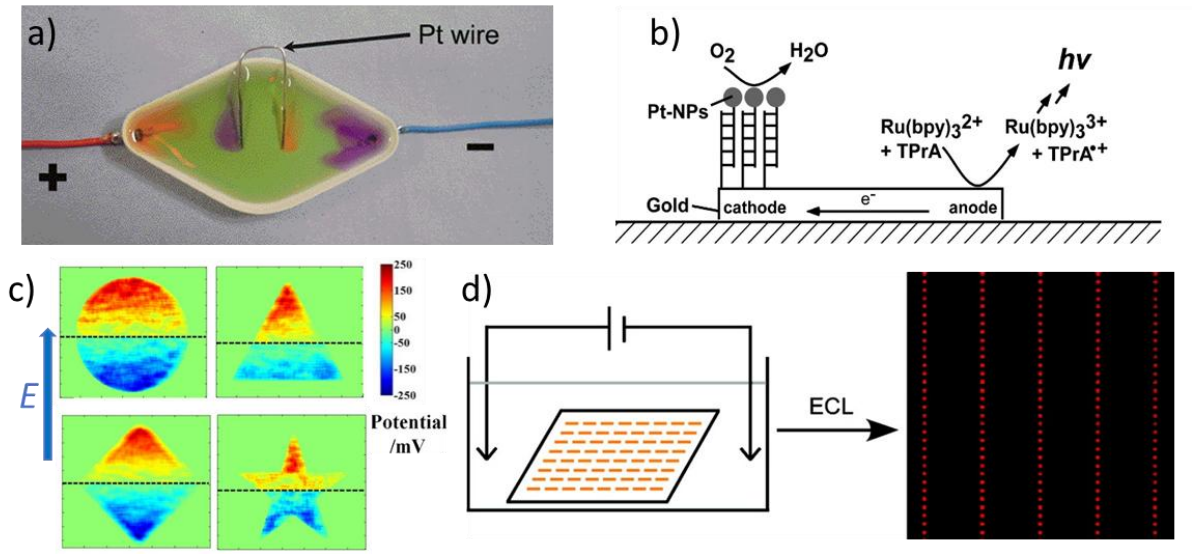

Figure 6. a) Colorimetric reading of the pH variations around the two "legs" of a BE (reproduced from ref. (177) with permission from the American Chemical Society). b) Schematic illustration of the working principle of the DNA sensing based on indirect bipolar ECL (reproduced from ref. (186) with permission from the American Chemical Society). c) SPRi images of BEs with different shapes showing the distribution of interfacial potential (adapted from ref. (202) with permission from the American Chemical Society). d) Wireless addressing of a large-scale BE array with ECL readout (adapted from ref. (195) with permission from the American Chemical Society).

The combination of BPE with ECL offers a great versatility to develop new sensing schemes for the detection of different analytes and biomolecules. Nucleic acids and biomarkers have been measured by original sensing strategies with a remarkable sensitivity (207-212). For example, cancer biomarkers have been detected on a closed indium-doped tin oxide (ITO) BE array biochip by parallel screening analysis with a simple visual ECL readout (209). Among the different analytical trends, paper-based bipolar ECL devices attracted great interest because they are versatile and inexpensive (213-220). However, the paper-based bipolar systems exhibit usually a higher resistance than classic metallic electrodes, leading to a lower sensitivity. To improve the conductivity and to enhance the ECL emission, various attempts have been made by integrating metallic nanoparticles and hybridization chain reaction amplification (214, 219, 221). In this context, Wang *et al.* introduced a novel potential-resolved paper-based biosensor for simultaneous detection of multiple microRNAs (222). A multiple-channel paper-based sensing microfluidic platform was prepared by wax-printing technology and Au nanoparticles were grown *in situ* to form areas with specific functions. Two ECL nano-emitters, CdTe quantum dots and Au@g-C_3N_4 nanosheets, generated ECL emission at different imposed potentials. This potential resolved emission decreased the interferences and led to low detection limits, typically down to the fM range. With the progress of BPE, more complex biological and analytical systems were investigated. Thus, bipolar methods have been used to capture cells (15, 223), as well as to measure specific

biomarkers at the single cell level by ECL (214, 224-228). Chen and co-workers exemplified an original approach based on a microfluidic chip with a transparent ITO BE for sensitive cell analysis. The detection of the level of folate receptors on a cell membrane was achieved due to the high affinity of the receptors to folic acid together with the quenching of ECL emission of the $[Ru(bpy)_3]^{2+}$/TPA system by folic acid (224). The same group broadened the applications of bipolar ECL for the cellular analysis by proposing several novel approaches (225, 229). Cancer cell surface proteins were labeled with ferrocene aptamers, which act as signal recognition and amplification probes (230). Both poles of the BEs were modified with amplification and recognition elements. On the cathodic side of the BE, Au nanoparticles were deposited to improve conductivity, enhance surface area, as well as to lower the overpotential for the reduction of dioxygen. The surface of the anodic side was modified by ferrocene aptamers through hybridization for detecting the amount of mucin-1 glycoprotein on MCF-7 (breast cancer) cells. The ECL signal was modulated by the efficient quenching of ECL by oxidized ferrocene (230). The analytical scheme with the signal quenching amplification allowed detection of 20 MCF-7 cells. As illustrated by Figure 7a, the general strategy for such sensitive detection is the immobilization of the cells on the recognition pole of the BE and this event is transduced on the sensing pole with an ECL readout, which was modulated (228).

Since the readout signal of bipolar ECL is the light emission, it offers the opportunity to tune the color of the emission, which is not a classical parameter in electrochemistry. Multicolor bipolar ECL was achieved by using ECL luminophores emitting at different wavelengths and with different redox potentials (231-234). As already mentioned, BPE induces a gradient of interfacial potentials along the BE with respect to the surrounding solution. In other words, different ECL-active species might be oxidized at different locations of the polarized conductive object. Multicolor potential-resolved ECL was reported in a solution containing $Ir(ppy)_3$ (with ppy = 2-phenylpyridine) and $[Ru(bpy)_3]^{2+}$ (231). Green and red emissions were generated locally as well as an intermediate yellow color in the spatial domain (i.e. potential domain) where both ECL emissions occur simultaneously. Hogan and co-workers exemplified the first multicolor bipolar ECL detection of heavy metal ions (Figure 7b) (232). In the presence of a heavy metal ion, the bipolar ECL emission onset potentials of both $Ir(ppy)_3$ and $[Ru(bpy)_3]^{2+}$ decrease depending on the relative ease of reduction of each species in the sensing reservoir. This original approach allowed the qualitative and quantitative detection of heavy metals in water. The same combination of ECL luminophores was used to build a multicolour ECL sensor for the measurements of the prostate-specific antigen (PSA) in human blood serum. PSA guided deposition of silver particles, which regulated the electronic conductivity of the BE (235). This approach could be extended to more complex mixtures with several ECL emitters using the spectral and spatial resolution offered by coupling BPE and ECL.

The imaging features provided by ECL readout open various possibilities for BPE such as multiplexing, microscopy, high throughput detection with a single image, etc. Zhang and co-workers demonstrated the monitoring of transient collision events of single Pt nanoparticles on a closed bipolar microelectrode (236). The electrocatalytic signal of a Pt nanoparticle

immobilized on the cathodic pole was coupled to the ECL emission on the anodic pole, generating a transient optical signal. The same group reported the use of a massive array of closed bipolar ultramicroelectrodes in an original imaging configuration.(237) The ordered array contained ca. 146,000 individual 8 µm-diameter carbon ultramicroelectrodes per cm², embedded in a 15 µm thick insulating and freestanding membrane (Figure 7c). Each ultramicroelectrode may generate ECL light individually on the anodic side and reflects the electrochemical activity occurring on the other side. Indeed, the reduction reactions on one side of the array are electrically coupled to an oxidative ECL process on the opposite side of the closed BE array. The entire array was recorded in a single image. It means that each ultramicroelectrode can be seen as a pixel forming the final ECL image and allows mapping of transient electrochemical processes. For example, Figure 7c (bottom) shows the progression of the ECL response during the depletion time lapse generated by a 50 µm Au microelectrode array positioned in the cathodic reservoir and close to the array. The system operated in a generator-collector mode. Similar array-based strategies have been reported for imaging various biological or physico-chemical activities, such as electrocatalysts, cells or the respiratory activity of cell spheroids (209, 238-242).

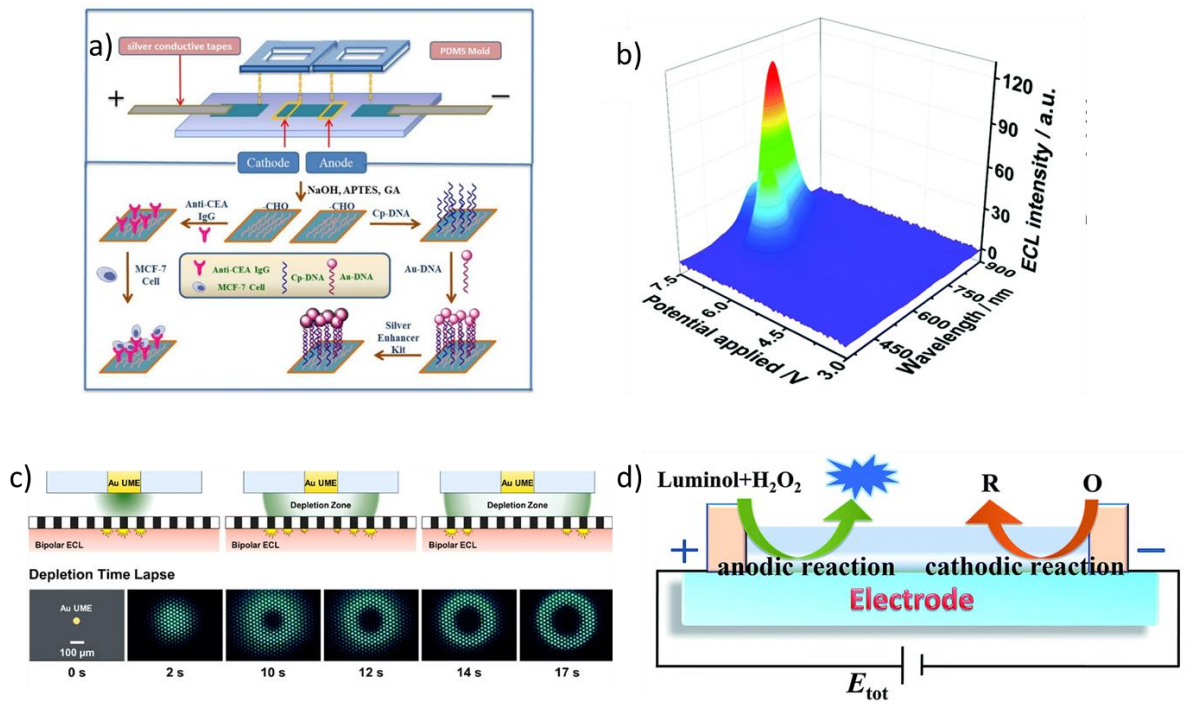

Figure 7. a) Schematic diagram and detection mechanism of the time-resolved ECL biosensor based on closed BEs (228), (reproduced with permission from the American Chemical Society). b) Potential resolved bipolar ECL emission 3D spectrum recorded in a mixture of $Ir(ppy)_3$ and $[Ru(bpy)_3]^{2+}$ (reproduced from ref. (232) with permission from the Royal Society of Chemistry). c) Schematic diagram showing the principle of the ECL imaging using a highly dense array of bipolar ultramicroelectrodes in a closed configuration with the imaging of a depletion zone in a generator-collector setup (reproduced from ref. (237) with permission from the American Chemical Society). d) ECL mechanism of a single-

electrode electrochemical system (reproduced from ref. (189) with permission from the Royal Society of Chemistry).

To improve the performances of bipolar ECL, different approaches have been reported by changing the sensing principle, the electrode material or the nature of the imposed potential signal. For example, Shannon and co-workers proposed square wave voltage excitation to trigger ECL detection (243). The autors demonstrated the working principle with a model analyte, $Fe(CN)_6^{3-}$, and a DNA proximity assay providing a detection limit of 300 fmol/cm^{-2}. Later, Anand and co-workers evaluated alternating current voltammetry with a smartphone as a photodetector (188). Their work showed that the alternating luminescence followed the current very accurately to enable quantitative sensing, but was however diminished at higher frequencies and shifting of the corresponding peaks. Xu and co-workers introduced a completely different strategy by coupling ECL with a diode (244, 245). The diode was utilized to rectify the alternating current efficiently and to enhance ECL detection. This wireless mini-device was able to detect both luminol and hydrogen peroxide with high sensitivity. Moreover, the wireless nature of the BPE was pushed further by developing remote addressing of the entire bipolar system or remote imaging of the ECL signal using modified optical fibers. In the first case, wireless energy transmission was used in an original manner to polarize the bipolar setup (246). This approach is promising for the development of portable or disposable ECL devices for various applications (e.g. point of care testing, field analysis, etc.). In the second case, dealing with double remote addressing and reading, an optical fiber, which was coated with a nanometer-thin gold film (i.e. semi-transparent) acted as a bipolar opto-electrode, on the one hand, to locally generate ECL in a wireless manner by BPE and on the other hand to guide the resulting ECL signal for remote imaging (247).

Instead of changing the imposed voltage excitation as mentioned above (188, 243), some groups proposed to manipulate the spatial distribution of the potential, which governs the BPE behavior in solution. Xu and co-workers exemplified the first single-electrode electrochemical system (SEES) based on a resistance loss mechanism at the level of the resistive electrode instead of the electrolyte solution, as usually performed in BPE (189). Indeed, the potential was imposed to a single resistive electrode and the potential drop occurs along its length. An ECL reporting reaction with luminol was used to map the potential distribution at the level of a SEES or of an electrode array. In this particular configuration, it is remarkable that the ECL signal is free from the ECL background problem from the feeder electrodes, which could be a major issue in classic bipolar ECL systems, even if very rarely mentioned in the literature. Another possibility to control the distribution and localization of the potential drop is offered by using spatial restrictions such as solid-state micropores or nanopipettes (248-254). Indeed, a sharp potential drop is focused at the level of the spatial restriction and not linearly spread in the solution, as in usual BPE configurations. The electric field strength is concentrated at the level of the restriction, which acts as the BE if fabricated with a conducting material. This enhanced local polarization was revealed by anodic ECL (255, 256). Light emission was confined in about half of the spatial restriction, which corresponds to the anodically-polarized region of the BE. Wireless polarization of small

conductive objects was achieved at much lower potentials than in a classic BPE approach (255). Jiang and co-workers exploited this sharp potential drop at the level of a nanopipette to perform intracellular wireless analysis of single cells by bipolar ECL (Figure 8a) (257). The inner walls of a nanopipette tip were first decorated by a Pt deposit that was used as an open BE configuration. The electric field provoked the sorting of various molecules from the intracellular space into the nanopipette, where they react with specific enzymes and produce ECL signals with luminol. This original method gives access to the intracellular concentrations of hydrogen peroxide, glucose as well as the intracellular sphingomyelinase activity (*i.e.* hydrolase). This strategy required a remarkably low voltage and minimized an eventual interference with the cell activity. Finally, it provided a novel concept in the field of single cell electrochemical analysis.

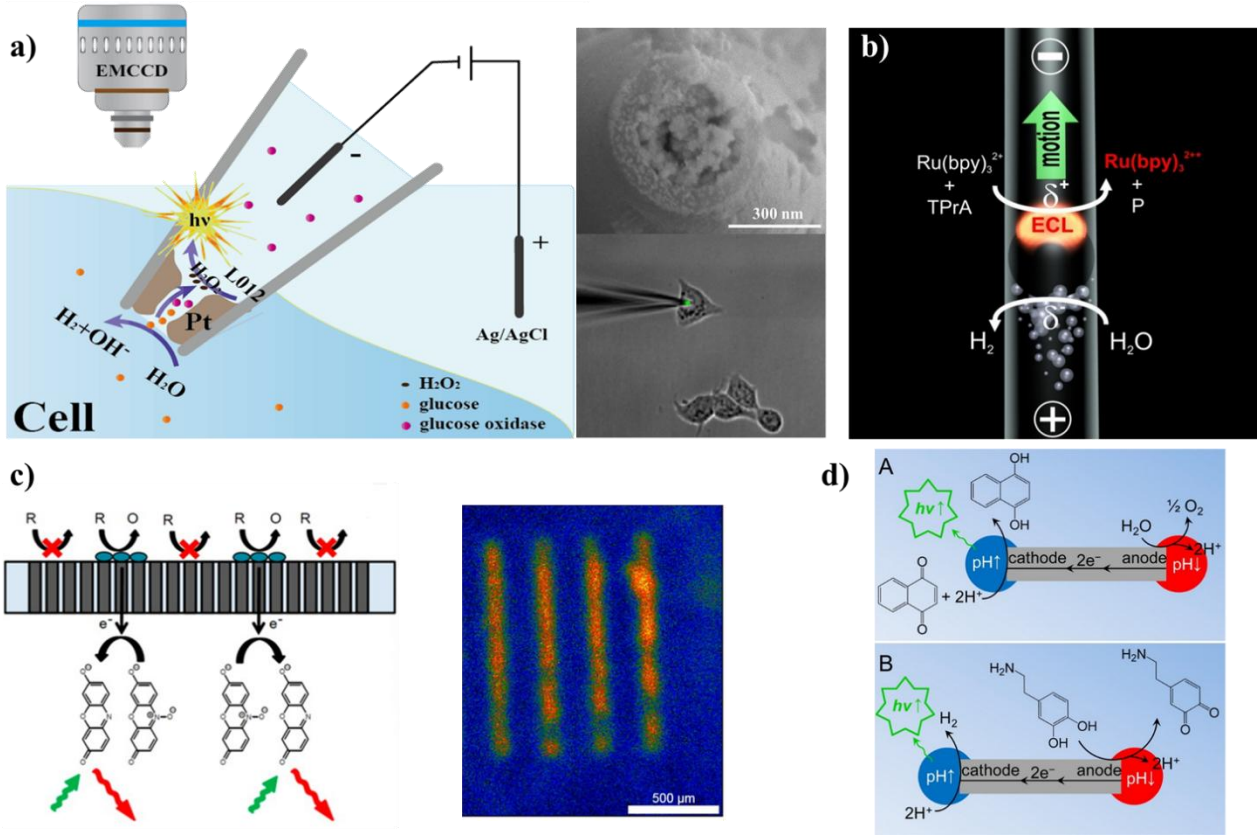

Figure 8. a) Scheme of the intracellular bipolar ECL detection at a nanopipette tip. The Pt-modified nanotip was inserted into the cytosol for intracellular wireless analysis. The insets show the SEM image of the Pt deposit at the nanopipette tip and the overlayed bright-field and ECL images of the nanopipette with the detection of intracellular glucose in a single living cell. The green spot is the ECL emission confined at the nanopipette tip (adapted from ref. (257) with permission from Wiley-VCH). b) Asymmetric bipolar ECL swimmer. The reduction of H_2O at the cathodic pole and oxidation of the ECL reagents at the anodic pole induces simultaneous motion and ECL emission of the bead in a capillary (reproduced from ref. (168) with permission from Wiley VCH). c) Scheme illustrating the basic principle of fluorescence-enabled electrochemical microscopy in a closed bipolar configuration with the

reduction of resazurin to resorufin (left). Image obtained by fluorescence-enabled bipolar electrochemical microscopy showing the oxidation of 10 mM H_2O_2 in 0.1 M NaOH at catalytically active "hot-spots" where Pt was deposited on a carbon fiber array (adapted from ref. (258) with permission from the American Chemical Society). d) Indirect visual detection of 1,4-naphthoquinone (A) and dopamine (B) by localized pH triggered fluorescence enhancement (reproduced from ref. (180) with permission from the American Chemical Society).

The versatility of BPE coupled to ECL allows imaging light-emitting bipolar objects in linear motion or rotation (259-261), or even generating both motion and light (168-170, 173). The dual electroactivity induced by BPE at the level of both poles of a polarized object was exploited to generate simultaneously its motion and ECL emission in a wireless manner (Figure 8b). A carbon bead was positioned in a vertical capillary between two feeder electrodes (168). The application of an electric field induced the propulsion of this bipolar object, which is based on the generation and release of hydrogen bubbles at the cathodic pole. Motion was produced in the direction opposite of the bubble release. Concomitantly, ECL emission was generated at the anodic pole by oxidation of $[Ru(bpy)_3]^{2+}$/TPA during the motion of the object. The light-emitting bipolar objects were called "ECL swimmers". ECL provides a direct monitoring of the object's motion, which is very useful in the context of autonomous swimmers (168, 262). Blue ECL emission with the luminol system was also reported with the specificity that ECL was generated on the same pole of the BE as well as the dioxygen bubbles inducing its linear motion (169). This approach was further explored for dynamic enzymatic glucose sensing (170). For instance, enzymatic ECL swimmers were developed where glucose dehydrogenase oxidized glucose to gluconolactone with the concomitant conversion of NAD^+ to NADH, which acted as a co-reactant in the ECL process. The oxidation of the $[Ru(bpy)_3]^{2+}$ luminophore and the enzymatically-produced NADH leads to ECL emission with a direct glucose-dependent light intensity. A concentration gradient of glucose was explored by the ECL swimmer and, as it was moving towards a region of higher glucose concentration, its ECL intensity increased (170). Such ECL-based sensing strategies, which combine in a synergetic way the wireless propulsion with the enzymatic selectivity at the level of moving objects opens the door to a new class of dynamic experiments with multifunctional objects.

While ECL provides remarkable analytical and imaging opportunities in combination with BPE, it requires the electrochemical reaction of specific reagents. To extend the scope of BPE, other visual readout methods have been proposed. Among them, fluorescence detection is one of the most important. Zhang and co-workers reported the use of fluorescence microscopy to image electrochemical and electrocatalytic activity on large bipolar arrays (Figure 8c) (258). The oxidation of a specific reagent (ferrocene, dopamine, or H_2O_2) was coupled to a fluorogenic reaction, the reduction of resazurin (weak emission) to resorufin (strong emission) (263-265). Therefore, the generation of this fluorescent product enabled the observation of the electrochemical kinetics and electrocatalytic heterogeneity over large bipolar electrochemical arrays. Xia and co-workers exploited this strategy using high-density

gold nanoelectrode arrays (266). Decreasing the size of the nanoelectrodes and increasing their density (*ca.* 7×10^9 electrodes/cm^2) should lead to a better optical resolution by limiting the diffusional overlap of the fluorogenic reporting reaction. In this fluorescence-based approach, the fluorescence emission was used for both quantification and imaging purposes as illustrated, for example, by the diffusion layers generated at BEs imaged by fluorescence microscopy (Figure 8d) (180, 267) or transient electrochemical and electrokinetic effects at nanoconfined BEs (268). Bohn and co-workers demonstrated the enhancement of the fluorescence reporting signal by redox cycling in nanopore recessed disk-multiscale BEs (269). High sensitivity was demonstrated by coupling self-induced redox cycling to fluorescence detection. Indeed, the reduction reaction of 1 nM of $[Ru(NH_3)_6]^{3+}$ on the nanoelectrode array was detected by measuring the fluorescence signal of the redox resazurin/resorufin system. Wang and co-workers designed a highly efficient fluorescence switch system based on a closed bipolar system (270). One pole of the BE was modified with gold nanoclusters, which acted as the fluorescent donor. The authors exploited the spectral overlap between the absorbance of an electrochromic material, Prussian blue, and the fluorescence spectrum of the gold nanoclusters to obtain a fluorescence switch between "on" and "off" states by changing the polarity of the imposed potential. This readout method could be extended to other electrically stimulable switches to develop memory materials, logic gates, and electrochemical sensors. Fluorescence microscopy was employed to monitor bipolar phenomena as reported recently by Crooks and co-workers (271). They tracked the redirection and separation of charged fluorescent microbeads within a bifurcated microelectrochemical device (271). The faradaic ion concentration polarization, triggered by imposing an adequate potential at a BE, results in the formation of an ion depletion zone and an ion enrichment zone. By controlling these zones, redirection and separation of ~100 % of the microbeads could be achieved. Recently, this work has been refined by reporting the concept of serial faradaic ion concentration polarization with two BEs used in series (272). Maksymiuk and co-workers introduced self-powered BEs with a fluorescence readout. First, they developed a simple self-powered BE system composed of an ion-selective pole (i.e. sensing pole) directly connected to the reporting pole, where a fluorescence reaction was produced. In other words, the potentiometric response of a K^+ ion-selective electrode (polypyrrole solid contact) was transformed into a fluorescence signal generated at the second remote pole (zinc electrode). The variations of the potassium cation concentration changed the membrane potential and modified the potential difference of the K^+ ion-selective electrode and zinc, which triggered reduction of the polypyrrole solid contact. This reaction was coupled with the oxidation of zinc (i.e. formation of zinc ions in solution), a process that can be monitored by fluorescence. The fluorescence signal was linearly dependent on the logarithm of activity of the analyte ions. However, a drawback of the first reported system was that the self-powered mode was operational only when the redox potential difference of reactions occurring at the opposite poles of the electrode was sufficiently high. In order to circumvent this limitation, the same group developed a system working spontaneously with two BEs, forming a cascade system (273). This approach was successfully applied to bipolar sensing based on the oxidation of L-ascorbic acid on a platinum electrode, connected with the reporting electrode coated by poly(3-octylthiophene), where reduction of the polymer results in formation of fluorescence species. The authors demonstrated also the measurement of

chloride anions with a similar fluorescence detection scheme (274). This series of reports is remarkable, because the transduction of the potentiometric signal into a fluorescence readout was achieved without any external power source.

Alternative optical readout methods have been combined with BPE to report the dual electroactivity of BEs. Amperometric and potentiometric sensing signals have been converted to a colorimetric output with closed BEs and arrays (275-278). For example, Bohn and co-workers developed a particular coulometric reporting scheme based on gold nanoaperture metamaterials prepared by nanosphere lithography (279). The transmission spectrum of metamaterials was altered by electrodissolution or electrodeposition of a dissimilar metal (i.e. Ag) in a 2-electrode closed bipolar electrochemical cell. This step modified the structure-based color of the metamaterial. Electrochromism was also successfully exploited to sense various analytes in a bipolar configuration (181, 182, 280-286). Wang and co-workers introduced a renewable display platform based on bipolar electrochromic readout for high-throughput screening applications (284). An electrochromic material such as the popular Prussian Blue was electrodeposited on the reporting pole of the BE, whereas the sensing pole was devoted to the loading of the catalyst. As already mentioned, considering the matching of the electrochemical activity on both poles, the color change was directly related to the amount and/or the activity of the catalysts. Fast imaging analysis of several electrocatalysts for methanol and ethanol oxidation was achieved with this approach.

5.3. Other readout schemes

As stated above, the anodic dissolution of a metal layer can be used as a readout to report another electrochemical reaction of interest that takes place at the cathodic pole of a BE. Such an approach was initially proposed by Chow *et al.* and demonstrated with silver metal as a proof-of-principle (126). In this work, a gold electrode was half-covered with a thin silver layer on the anodic side. In parallel, the cathodic pole was modified with a single-stranded DNA probe. After recognition with the DNA target and coupling with an enzymatic system, the process at the cathode triggers the permanent dissolution of Ag that is easily detectable. The readout reaction starts at the border of the BE before extending gradually towards the centre. The bipolar reactions stop when the BE has been sufficiently shortened so that the polarisation effect of the electric field becomes too weak to couple the oxidation of silver with the reduction process. This represents a change of paradigm since the final size directly reveals the electrochemical history experienced by the BE (i.e. charge or number of electrons involved). This original concept was latter updated by the same group with a series of improvements that enable the optimisation of the initial idea, transforming it into a very robust and versatile platform used for the testing of electrocatalysts (127, 287, 288). For the second generation of BEs, the uniform silver layer was replaced by an array of parallel microbands. This smart change offers an outstanding improvement of the readout since one has just to count the number of remaining stripes at the end of a given experiment (287). This facilitates the comparison of several electrocatalysts, as well as to easily follow the kinetics of the electrochemical processes. This configuration was used to compare the catalytic activity of Pt, Au, and ITO for the electrochemical reduction of molecular oxygen. Since

these materials exhibit a different onset potential for the investigated reaction, the most efficient catalyst, which is Pt, leads to the dissolution of a larger number of microbands. Again, a key advantage of BPE is the possibility to test in parallel various catalysts by simultaneously addressing several BEs with a single voltage source. The next step was to adapt the approach in order to test a larger amount of electrocatalysts and this led to the replacement of silver by another more appropriate metal. The reason is due to the large overpotential that is necessary to drive silver oxidation, as it is a rather noble metal. Therefore, the use of silver only allows to discriminate electrocatalysts that offer a very distinct electroactivity. However, when comparing for example very similar metal alloys, it is not possible anymore to distinguish their respective efficiency. Therefore, Ag was replaced by Cr, which requires a lower overpotential (127). An array of Cr microbands was used to compare the activity of bimetallic mixtures for hydrogen evolution reaction (HER). Pd metal was combined with either Au, Co or W with variable ratios. The number of Cr stripes remaining after applying the driving voltage for a given time was employed as a readout in order to identify the best chemical composition and stoichiometry. This approach was implemented to enable large scale fabrication of BE arrays as well as an automated deposition of the electrocatalyst precursors with a robotised arm equipped with piezo-dispensers. This enables high throughput screening of a large number of electrocatalysts in only a few minutes (288) as demonstrated in the case of HER with bi- and trimetallic combinations of metals. The screening was performed in several media by testing both neutral and acidic electrolytes. Again, the method results in a permanent record of the individual electrocatalytic performance that can be monitored either *in situ* or as an end-point reading. Moreover, video frames can be recorded during the dissolution of the Cr microbands, allowing the access to kinetics data.

Another completely different readout strategy was proposed more recently. It is based on the deformation of a BE, made out of a conducting polymer, that will bend more or less strongly in the presence or absence of a given chemical target. In other words, the BE is used as a sort of cantilever that is actuated to report quantitatively an electrochemical process (183, 289). Indeed, such a device can be considered as an electromechanical readout of a given chemical information since the degree of deformation correlates with the amount of electroactive analyte that is present in solution. This was first illustrated with the detection of glucose by taking advantage of an electro-enzymatic approach with glucose oxidase (183). The concept was exemplified by using a freestanding polymer film made out of polypyrrole. The conducting polymer is immobilized on an inert support and directly used as a BE. The oxidation of the analyte occurs at the positively polarized extremity, whereas the electrons are shuttled towards the cathodic side that is used as a cantilever. The electrochemical reduction of polypyrrole is accompanied by the doping of the film through the insertion of counterions. This leads to a swelling of the polymer film that ultimately bends at the macroscopic level. The resulting actuation appears to be proportional to the glucose concentration, thus providing an unconventional electroenzymatic assay. The approach has then been extended to the detection of chiral analytes by using hybrid cantilevers composed of polypyrrole and a

chiral imprinted mesoporous platinum layer (289). The metal layer is the active site where enantioselective oxidation occurs (290-292), whereas the polymer extremity is again reduced and therefore starts to bend when the appropriate enantiomer is present in solution. Finally, the concept was proven to be able to achieve also absolute chiral discrimination by integrating an inherently chiral oligomer in such a device (293). The polypyrrole cantilever was modified with a chiral oligo-dibenzothiophene moiety which features an atropoisomeric core and can be obtained in an enantiopure form, enabling the preparation of a cantilever capable of chiral discrimination. Again, the freestanding hybrid polymer film can be addressed in a wireless way by means of BPE. This time, the bending exclusively occurs in the presence of one enantiomer and absolutely not when its antipode is present. This concept has been validated with the specific chiral detection of L- and D-DOPA (3,4-dihydroxyphenylalanine) by using either the S- or the R-form of the oligomer, respectively. As previously, the degree of bending depends directly on the DOPA concentration.

6. Conclusion and perspectives

The goal of this chapter was to give the reader a general introduction into the basic concepts of BPE, accompanied by a non-exhaustive description of some classic, as well as more recent examples of developments. Indeed, many novel and rather unconventional approaches have been reported in the literature over the last few years, being often very different in terms of set-up and envisioned applications compared to the experiments that have been carried out a few decades ago.

We have discussed here only a small, but representative selection of such experiments based on the very general concept of BPE. We tried to illustrate that, no matter whether it is in the frame of materials science, analytical chemistry or some less common aspects like the controlled generation of motion or actuation, the use of BPE brings in most of the cases an added value to the system when compared to other electrochemical approaches. Obviously, there are also some drawbacks, like the fact that sometimes rather high electric fields have to be used or that reactions at the feeder electrodes can considerably disturb these experiments. However, in many cases it is possible to circumvent these problems by adapting the experimental set-up in the right way.

As a result, the number of scientists using this concept in various areas of chemistry is constantly increasing every year, as can be seen from the related publication statistics, and this is essentially due to the following specific advantages:

1. The experiments do not need a direct physical contact with the object that will act as a BE. This wireless character is without any doubt the most attractive feature and enables many experiments that absolutely cannot be done by using classic electrochemical approaches.

2. A direct result of the previous point is the fact that the technique allows performing redox reactions on thousands or even millions of objects simultaneously, with just one pair of

feeder electrodes providing the driving force. This also gives the possibility to address moving objects, thus enabling for example the design of mechano-electrochemical devices.

3. By definition, BPE is a very adequate tool for breaking the symmetry of chemical systems, thus providing new opportunities in various fields, ranging from the triggering of directional motion to the synthesis of surface gradients and other asymmetric or multifunctional materials.

4. A last, more extra-scientific argument is the fact that BPE experiments are rather easy to implement, as they require only simple and cheap instrumentation, which can be handled even by inexperienced persons.

One can expect that for all these reasons the number of applications of the concept will still continue to grow in the near future, certainly within the field of chemistry, but most likely also in neighboring areas such as biology, and we hope that this chapter might contribute to the

References

1. Bard, A.J. and Faulkner, L.R. (2001). Electrochemical methods. 2nd edition. John Wiley & Sons, Inc.
2. Hiddleston, J.N. and Douglad, A.F. (1968). Fluidized Bed Electrodes- Fundamental Measurements and Implications. Nature 218: 601–602.
3. van der Heiden, C.M., Raats, S.M., Boon, J.F. (1978). Fluidised Bed Electrolysis for Removal or Recovery of Metals from Dilute Solutions. Chemistry and Industry 1: 465–468.
4. Fleischmann, M., Goodridge, F., King, C.J.H. (1978). Electrochemical processes. US Patent 4,124,453.
5. Loget, G., Zigah, D., Bouffier, L., Sojic, N., Kuhn, A. (2013). Bipolar Electrochemistry: From Materials Science to Motion and Beyond. Accounts of Chemical Research 46: 2513–2523.
6. Fosdick, S.E., Knust, K.N., Scida, K., Crooks, R.M. (2013). Bipolar Electrochemistry. Angewandte Chemie International Edition 52 (40): 10438–10456.
7. Shida, N., Zhou, Y., Inagi, S. (2019). Bipolar Electrochemistry: A Powerful Tool for Electrifying Functional Material Synthesis. Accounts of Chemical Research 52 (9): 2598–2608.
8. Koefoed, L., Pedersen, S.U., Daasbjerg, K. (2017). Bipolar electrochemistry–A wireless approach for electrode reactions. Current Opinion in Electrochemistry 2 (1): 13–17.
9. Sequeira, C.A.C., Cardoso, D.S.P., Gameiro, M.L.F. (2016). Bipolar Electrochemistry, a Focal Point of Future Research. Chemical Engineering Communications 203 (8): 1001–1008.
10. Loget, G. and Kuhn, A. (2011). Shaping and exploring the micro- and nanoworld using bipolar electrochemistry. Analytical and Bioanalytical Chemistry 400 (6): 1691–1704.
11. Karimian, N., Hashemi, P., Afkhami, A., Bagheri, H. (2019). The principles of bipolar electrochemistry and its electroanalysis applications. Current Opinion in Electrochemistry 17: 30–37.
12. Pébère, N. and Vivier, V. (2016). Local Electrochemical Measurements in Bipolar Experiments for Corrosion Studies. ChemElectroChem 3 (3): 415–421.
13. Munktell, S., Tydén, M., Högström, J., Nyholm, L., Björefors, F. (2013). Bipolar electrochemistry for high-throughput corrosion screening. Electrochemistry Communications 34: 274–277.
14. Zhou, Y. and Engelberg, D.L. (2020). Fast testing of ambient temperature pitting corrosion in type 2205 duplex stainless steel by bipolar electrochemistry experiments. Electrochemistry Communications 117: 106779.

15. Li, M. and Anand, R.K. (2017). High-Throughput Selective Capture of Single Circulating Tumor Cells by Dielectrophoresis at a Wireless Electrode Array. Journal of the American Chemical Society 139 (26): 8950–8959.
16. Fleischmann, M., Ghoroghchian, J., Pons, S. (1985). Electrochemical behavior of dispersions of spherical ultramicroelectrodes. 1. Theoretical considerations. The Journal of Physical Chemistry 89 (25): 5530–5536.
17. Fleischmann, M., Ghoroghchian, J., Rolison, D., Pons, S. (1986). Electrochemical behavior of dispersions of spherical ultramicroelectrodes. The Journal of Physical Chemistry 90 (23): 6392–6400.
18. Comninellis, C., Plattner, E., Bolomey, P. (1991). Estimation of current bypass in a bipolar electrode stack from current-potential curves. Journal of Applied Electrochemistry 21 (5): 415–418.
19. Saakes, M., Woortmeijer, R., Schmal, D. (2005). Bipolar lead–acid battery for hybrid vehicles. Journal of Power Sources 144 (2): 536–545.
20. Marsh, R.A., Russell, P.G., Reddy, T.B. (1997). Bipolar lithium-ion battery development. Journal of Power Sources 65 (1–2): 133–141.
21. Karami, H., Mousavi, M.F., Shamsipur, M., Riahi, S. (2006). New dry and wet Zn-polyaniline bipolar batteries and prediction of voltage and capacity by ANN. Journal of Power Sources 154 (1): 298–307.
22. Hermann, A., Chaudhuri, T., Spagnol, P. (2005). Bipolar plates for PEM fuel cells: A review. International Journal of Hydrogen Energy 30 (12): 1297–1302.
23. Sudoh, M., Kodera, T., Hino, H., Shimamura, H. (1988). Effect of anodic and cathodic reactions on oxidative degradation of phenol in an undivided bipolar electrolyser. Journal of Chemical Engineering of Japan 21 (2): 198–203.
24. Hänni, W., Perret, A., Comninellis, C. (2001). Electrolytic cell with bipolar electrode including diamond. US Patent 6,306,270 B1.
25. Alkire, R.C., Engelmaier, W., Kessler, T.J. (1977). Electrolytic cell with bipolar electrodes. US Patent 4,043,891.
26. Bradley, J.-C., Crawford, J., McGee, M., Stephens, S.G. (1998). A Contactless Method for the Directed Formation of Submicrometer Copper Wires. Journal of the Electrochemical Society 145 (3): L45–L47.
27. Bradley, J.-C., Babu, S., Ndungu, P. (2005). Contactless tip-selective electrodeposition of palladium onto carbon nanotubes and nanofibers. Fullerenes, Nanotubes, Carbon Nanostructures 13: 227–237.
28. Bradley, J.-C. and Ma, Z. (1999). Contactless Electrodeposition of Palladium Catalysts. Angewandte Chemie International Edition 38 (11): 1663–1666.
29. Bradley, J.-C., Chen, H.-M., Crawford, J., Eckert, J., Ernazarova, K., Kurzeja, T., et al. (1997). Creating electrical contacts between metal particles using directed electrochemical growth. Nature 389 (6648): 268–271.
30. Bradley, J.-C., Ma, Z., Stephens, S.G. (1999). Electric Field Directed Construction of Diodes Using Free-standing Three-dimensional Components. Advanced Materials 11 (5): 374–378.
31. Loget, G. and Kuhn, A. (2013). Bipolar electrochemistry in the nanosciences. In: Specialist Periodical Reports Electrochemistry (Compton, R.G. and Wadhawans, J.D., editors.), 71–103.
32. Bouffier, L., Arbault, S., Kuhn, A., Sojic, N. (2016). Generation of electrochemiluminescence at bipolar electrodes: concepts and applications. Analytical and bioanalytical chemistry 408: 7003–7011.
33. Bouffier, L., Manojlovic, D., Kuhn, A., Sojic, N. (2019) Advances in bipolar electrochemiluminescence for the detection of biorelevant molecular targets. Current Opinion in Electrochemistry 16: 28–34.
34. Kuhn, A., Sojic, N., Zigah, D., Bouffier, L. (2017). Recent Advances in Bipolar Electrochemistry. In: Electroanalytical Chemistry; A Series of Advances. 1st edition. (Bard, A.J. and Zoski, C.G., editors, Taylor & Francis).

35. Bouffier, L., Sojic, N., Kuhn, A. (2019). Biochemical sensing based on bipolar electrochemistry. In: Bioelectrochemistry. (Cosnier, S., editor, De Gruyter). p. 101–120.
36. Kuhn, A., Crooks, R.M., Inagi, S. (2016). A Compelling Case for Bipolar Electrochemistry. ChemElectroChem 3 (3): 351–352.
37. Rahn, K.L. and Anand, R.K. (2021). Recent Advancements in Bipolar Electrochemical Methods of Analysis. Analytical Chemistry 93 (1): 103–123.
38. Duval, J., Kleijn, J.M., van Leeuwen, H.P. (2001). Bipolar electrode behaviour of the aluminium surface in a lateral electric field. Journal of Electroanalytical Chemistry 505 (1–2): 1–11.
39. Bouffier, L., Zigah, D., Sojic, N., Kuhn, A. (2021). Bipolar (bio)electroanalysis. Annual Review of Analytical Chemistry in press.
40. Deng, H., Stockmann, T.J., Peljo, P., Opallo, M., Girault, H.H. (2014). Electrochemical oxygen reduction at soft interfaces catalyzed by the transfer of hydrated lithium cations. Journal of Electroanalytical Chemistry 731: 28–35.
41. Rodgers, A.N.J. and Dryfe; R.A.W. (2016). Oxygen Reduction at the Liquid–Liquid Interface: Bipolar Electrochemistry through Adsorbed Graphene Layers. ChemElectroChem 3 (3): 472–479.
42. Toth, P.S., Rodgers, A.N.J., Rabiu, A.K., Dryfe, R.A.W. (2015). Electrochemical activity and metal deposition using few-layer graphene and carbon nanotubes assembled at the liquid–liquid interface. Electrochemistry Communications 50: 6–10.
43. Toth, P.S., Ramasse, Q.M., Velický, M., Dryfe, R.A.W. (2015). Functionalization of graphene at the organic/water interface. Chemical Science 6 (2): 1316–1323.
44. Delgado, A.V., González-Caballero, F., Hunter, R.J., Koopal, L.K., Lyklema, J. (2007). Measurement and interpretation of electrokinetic phenomena. Journal of Colloid and Interface Science 309 (2): 194–224.
45. Duval, J.F.L., Huijs, G.K., Threels, W.F., Lyklema, J., van Leeuwen, H.P. (2003). Faradaic depolarization in the electrokinetics of the metal–electrolyte solution interface. Journal of Colloid and Interface Science 260 (1): 95–106.
46. Dumitrescu, I., Anand, R.K., Fosdick, S.E., Crooks, R.M. (2011). Pressure-Driven Bipolar Electrochemistry. Journal of the American Chemical Society 133 (13): 4687–4689.
47. Kusakabe, K., Morooka, S., Kato, Y. (1982). Current paths and electrolysis efficiency in bipolar packed-bed electrodes. Journal of Chemical Engineering of Japan 15 (1): 45–50.
48. Plimley, R.E. and Wright, A.R. (1984). A bipolar mechanism for charge transfer in a fluidised bed electrode. Chemical Engineering Science 39 (3): 395–405.
49. Kazdobin, K., Shvab, N., Tsapakh, S. (2000). Scaling-up of fluidized-bed electrochemical reactors. Chemical Engineering Journal 79 (3): 203–209.
50. Loget, G., Roche, J., Kuhn, A. (2012). True bulk synthesis of Janus objects by bipolar electrochemistry. Advanced Materials 24: 5111–5116.
51. Ordeig, O., Godino, N., del Campo, J., Muñoz, F.X., Nikolajeff, F., Nyholm, L. (2008). On-Chip Electric Field Driven Electrochemical Detection Using a Poly(dimethylsiloxane) Microchannel with Gold Microband Electrodes. Analytical Chemistry 80 (10): 3622–3632.
52. Warakulwit, C., Nguyen, T., Majimel, J., Delville, M.-H., Lapeyre, V., Garrigue, P., et al. Dissymmetric Carbon Nanotubes by Bipolar Electrochemistry. Nano Letters 8 (2): 500–504.
53. Perro, A., Reculusa, S., Ravaine, S., Bourgeat-Lami, E., Duguet, E. (2005). Design and synthesis of Janus micro- and nanoparticles. Journal of Materials Chemistry 15 (35-36): 3745–3760.
54. Roh, K.-H., Martin, D.C., Lahann, J. (2005). Biphasic Janus particles with nanoscale anisotropy. Nature Materials 4 (10): 759–763
55. Ongaro, M., Gambirasi, A., Favaro, M., Kuhn, A., Ugo, P. (2014). Asymmetrical modification of carbon microfibers by bipolar electrochemistry in acetonitrile. Electrochimica Acta 116: 421–428.
56. Loget, G., Larcade, G., Lapeyre, V., Garrigue, P., Warakulwit, C., Limtrakul, J., et al. Single point electrodeposition of nickel for the dissymmetric decoration of carbon tubes. Electrochimica Acta 55 (27): 8116–8120.

57. Fattah, Z., Garrigue, P., Lapeyre, V., Kuhn, A., Bouffier, L. (2012). Controlled Orientation of Asymmetric Copper Deposits on Carbon Microobjects by Bipolar Electrochemistry. The Journal of Physical Chemistry C 116 (41): 22021–22027.
58. Tisserant, G., Fattah, Z., Ayela, C., Roche, J., Bernard, P., Zigah, D., et al. (2015). Generation of metal composition gradients by means of bipolar electrodeposition. Electrochimica Acta 179: 276–281.
59. Fattah, Z., Garrigue, P., Goudeau, B., Lapeyre, V., Kuhn, A., Bouffier, L. (2013). Capillary Electrophoresis as a Production Tool for Asymmetric Microhybrids. Electrophoresis 34: 1985–1990.
60. Loget, G., Lapeyre, V., Garrigue, P., Warakulwit, C., Limtrakul, J., Delville, M.-H., et al. Versatile Procedure for Synthesis of Janus-Type Carbon Tubes. Chemistry of Materials 23 (10): 2595–2599.
61. Ramaswamy, R. and Shannon, C. (2011). Screening the Optical Properties of Ag−Au Alloy Gradients Formed by Bipolar Electrodeposition Using Surface Enhanced Raman Spectroscopy. Langmuir 27 (3): 878–881.
62. Ramakrishnan, S., Shannon, C. (2010). Display of Solid-State Materials Using Bipolar Electrochemistry. Langmuir 26 (7): 4602–4606.
63. Xu, F., Wang, H., He, X.-D., Deng, N., Li, F., Li, B., et al. One-step deposition of NixCu1−x alloys with both composition gradient and morphology evolution by bipolar electrochemistry. Journal of Electroanalytical Chemistry 823: 213–220.
64. Termebaf, H., Shayan, M., Kiani, A. (2015). Two-Step Bipolar Electrochemistry: Generation of Composition Gradient and Visual Screening of Electrocatalytic Activity. Langmuir 31 (48): 13238–13246.
65. Wang, B., Yu, S., Shannon, C. (2020). Reduction of 4-Nitrothiophenol on Ag/Au Bimetallic Alloy Surfaces Studied Using Bipolar Raman Spectroelectrochemistry. ChemElectroChem 7 (10): 2236–2241.
66. Liu, J.-J., Yang, X.-F., Li, F., Yang, Z., Xie, J., Li, Y., et al. (2019). Area-Step Cyclic Voltammetry for Assessing Local Electrocatalytic Activity of Gradient Materials. ChemElectroChem 6 (20): 5237–5241.
67. Tisserant, G., Gillion, J., Lannelongue, J., Fattah, Z., Garrigue, P., Roche, J., et al. (2016). Single-Step Screening of the Potential Dependence of Metal Layer Morphologies along Bipolar Electrodes. ChemElectroChem 3 (3): 387–391.
68. Lundgren, A., Munktell, S., Lacey, M., Berglin, M., Björefors, F. (2016). Formation of Gold Nanoparticle Size and Density Gradients via Bipolar Electrochemistry. ChemElectroChem 3 (3): 378–382.
69. Li, Y., Dong, Y., Yang, Y., Yu, P., Zhang, Y., Hu, J., et al. (2019). Rational Design of Silver Gradient for Studying Size Effect of Silver Nanoparticles on Contact Killing. ACS Biomaterials Science & Engineering 5 (2): 425–431.
70. Zuccaro, L., Kuhn, A., Konuma, M., Yu, H.K., Kern, K., Balasubramanian, K. (2016). Selective Functionalization of Graphene Peripheries by using Bipolar Electrochemistry. ChemElectroChem 3 (3): 372–377.
71. Kayran, Y.U., Eßmann, V., Grützke, S., Schuhmann, W. (2016). Selection of Highly SERS-Active Nanostructures from a Size Gradient of Au Nanovoids on a Single Bipolar Electrode. ChemElectroChem 3 (3): 399–403.
72. Dorri, N., Shahbazi, P., Kiani, A. (2014). Self-Movement of Water Droplet at the Gradient Nanostructure of Cu Fabricated Using Bipolar Electrochemistry. Langmuir 30 (5): 1376–1382.
73. Roche, J., Loget, G., Zigah, D., Fattah, Z., Goudeau, B., Arbault, S., et al. (2014). Straightforward synthesis of ringed particles. Chemical Science 5: 1961–1966.
74. Braun, T.M. and Schwartz, D.T. (2015). Localized Electrodeposition and Patterning Using Bipolar Electrochemistry. Journal of the Electrochemical Society 162 (4): D180–D185.

75. Braun, T.M. and Schwartz, D.T. (2016). Remote Control Electrodeposition: Principles for Bipolar Patterning of Substrates without an Electrical Connection. Journal of the Electrochemical Society 163 (12): D3014–D3019.
76. Braun, T.M. and Schwartz, D.T. (2019). Exploring the Kinetic and Thermodynamic Relationship of Charge Transfer Reactions Used in Localized Electrodeposition and Patterning in a Scanning Bipolar Cell. Frontiers in chemistry 7: 340.
77. Bradley, J.-C., Crawford, J., Ernazarova, K., McGee, M., Stephens, S.G. (1997). Wire formation on circuit boards using spatially coupled bipolar electrochemistry. Advanced Materials 9 (15): 1168–1171.
78. Sanjuan-Alberte, P., Saleh, E., Shaw, A.J., Lacalendola, N., Willmott, G., Vaithilingam, J., et al. (2019). Remotely Controlled in Situ Growth of Silver Microwires Forming Bioelectronic Interfaces. ACS Applied Materials & Interfaces 11 (9): 8928–8936.
79. Koizumi, Y., Nishiyama, H., Tomita, I., Inagi, S. (2018). Templated bipolar electrolysis for fabrication of robust Co and Pt nanorods. Chemical Communications 54 (74): 10475–10478.
80. Zhou, Y., Shida, N., Koizumi, Y., Endo, K., Tomita, I., Inagi, S. (2020). Fabrication of One-Dimensional Polymer Nanowires by Templated Bipolar Electropolymerization Promoted by Electrophoretic Effect. Macromolecules 53 (18): 8123–8130.
81. Malytska, I., Doneux, T., Bougouma, M., Kuhn, A., Bouffier, L. (2019). Wireless Addressing of Freestanding MoSe2 Macro- and Microparticles by Bipolar Electrochemistry. The Journal of Physical Chemistry C 123 (9): 5647–5652.
82. Malytska, I., Mézière, C., Kielar, M., Hirsch, L., Wantz, G., Avarvari, N., et al. (2017). Bipolar Electrochemistry with Organic Single Crystals for Wireless Synthesis of Metal–Organic Janus Objects and Asymmetric Photovoltage Generation. The Journal of Physical Chemistry C 121 (23): 12921–12927.
83. Mukherjee, S., Libisch, F., Large, N., Neumann, O., Brown, L.V., Cheng, J., et al. (2013). Hot Electrons Do the Impossible: Plasmon-Induced Dissociation of H2 on Au. Nano Letters 13 (1): 240–247.
84. Ongaro, M., Roche, J., Kuhn, A., Ugo, P. (2014). Asymmetric modification of TiO2 nanofibers with gold by electric-field-assisted photochemistry. ChemElectroChem 1: 2048–2051.
85. Tiewcharoen, S., Warakulwit, C., Lapeyre, V., Garrigue, P., Fourier, L., Elissalde, C., et al. (2017). Anisotropic Metal Deposition on TiO2 Particles by Electric-Field-Induced Charge Separation. Angewandte Chemie International Edition 56 (38): 11431–11435.
86. Melvin, A.A., Lebraud, E., Garrigue, P., Kuhn, A. (2020). Light and electric field induced unusual large-scale charge separation in hybrid semiconductor objects. Physical Chemistry Chemical Physics 22 (39): 22180–22184.
87. Ongaro, M., Gambirasi, A., Ugo, P. (2016). Closed Bipolar Electrochemistry for the Low-Potential Asymmetrical Functionalization of Micro- and Nanowires. ChemElectroChem 3 (3): 450–456.
88. Koizumi, Y., Shida, N., Ohira, M., Nishiyama, H., Tomita, I., Inagi, S. (2016). Electropolymerization on wireless electrodes towards conducting polymer microfibre networks. Nature Communications 7: 10404.
89. Buzzeo, M.C., Evans, R.G., Compton, R.G. (2004). Non-Haloaluminate Room-Temperature Ionic Liquids in Electrochemistry–A Review. ChemPhysChem 5 (8): 1106–1120.
90. Kong, S., Fontaine, O., Roche, J., Bouffier, L., Kuhn, A., Zigah, D. (2014). Electropolymerization of Polypyrrole by Bipolar Electrochemistry in an Ionic Liquid. Langmuir 30 (11): 2973–2976.
91. Kumsapaya, W., Bakaï, M.-F., Loget, G., Goudeau, B., Warakulwit, C., Limtrakul, J., et al. (2013). Janus Beads obtained by Grafting of Organic Layers via Bipolar Electrochemistry. Chemistry – A European Journal 19 (5): 1577–1580.
92. Kumsapaya, C., Limtrakul, J., Kuhn, A., Zigah, D., Warakulwit, C. (2016). Bipolar Electrografting on the Inner Wall of Carbon Nanotubes. ChemElectroChem 3: 410–414.

93. Koefoed, L., Pedersen, S. U., Daasbjerg, K., Kuhn, A., Zigah, D. (2016). Bifunctional Substrates Obtained by Bipolar Electrochemistry of 4-aminoethylbenzenediazonium. RSC Advances 6: 3882–3887.
94. Koefoed, L., Pedersen, S.U., Daasbjerg, K. (2016). Grafting of Aryl Diazonium, Iodonium, and Sulfonium Salts in Unusual Patterns by Exploiting the Potential Gradient in Bipolar Electrochemistry. ChemElectroChem 3 (3): 495–501.
95. Koefoed, L., Pedersen, E.B., Thyssen, L., Vinther, J., Kristiansen, T., Pedersen, S.U., et al. (2016). Functionalizing Arrays of Transferred Monolayer Graphene on Insulating Surfaces by Bipolar Electrochemistry. Langmuir 32 (25): 6289–6296.
96. Madsen, M.R., Koefoed, L., Jensen, H., Daasbjerg, K., Pedersen, S.U. (2019). Two-phase bipolar electrografting. Electrochimica Acta 317: 61–69.
97. Zhou, Y., Shida, N., Koizumi, Y., Watanabe, T., Nishiyama, H., Tomita, I., et al. (2019). Template-free perpendicular growth of a poly(3,4-ethylenedioxythiophene) fiber array by bipolar electrolysis under an iterative potential application. Journal of Materials Chemistry C 7 (46): 14745–14751.
98. Loget, G., Roche, J., Gianessi, E., Bouffier, L., Kuhn, A. (2012). Indirect bipolar electrodeposition. Journal of the American Chemical Society 134 (49): 20033–20036.
99. Niamlaem, M., Phuakkong, O., Garrigue, P., Goudeau, B., Ravaine, V., Kuhn, A., et al. (2020). Asymmetric Modification of Carbon Nanotube Arrays with Thermoresponsive Hydrogel for Controlled Delivery. ACS Applied Materials & Interfaces 12 (20): 23378–23387.
100. Fattah, Z.A., Bouffier, L., Kuhn, A. (2017). Indirect bipolar electrodeposition of polymers for the controlled design of zinc microswimmers. Applied Materials Today 9: 259–265.
101. Yadnum, S., Roche, J., Lebraud, E., Negrier, P., Garrigue, P., Bradshaw, D., et al. (2014). Site-Selective Synthesis of Janus- type Metal-Organic Framework Composites. Angewandte Chemie-International Edition 53 (15): 4001–4005.
102. Tornøe, C.W., Christensen, C., Meldal, M. (2002). Peptidotriazoles on Solid Phase: [1,2,3]-Triazoles by Regiospecific Copper(I)-Catalyzed 1,3-Dipolar Cycloadditions of Terminal Alkynes to Azides. The Journal of Organic Chemistry 67 (9): 3057–3064.
103. Shida, N., Ishiguro, Y., Atobe, M., Fuchigami, T., Inagi, S. (2012). Electro-Click Modification of Conducting Polymer Surface Using Cu(I) Species Generated on a Bipolar Electrode in a Gradient Manner. ACS Macro Letters 1 (6): 656–659.
104. Ino, K., Matsumoto, T., Taira, N., Kumagai, T., Nashimoto, Y., Shiku, H. (2018). Hydrogel electrodeposition based on bipolar electrochemistry. Lab on a Chip 18 (16): 2425–2432.
105. Fattah, Z., Roche, J., Garrigue, P., Zigah, D., Bouffier, L., Kuhn, A. (2013). Chemiluminescence from Asymmetric Inorganic Surface Layers Generated by Bipolar Electrochemistry. ChemPhysChem 14 (10): 2089–2093.
106. Magenau, A.J., Strandwitz, N.C., Gennaro, A., Matyjaszewski, K. (2011). Electrochemically mediated atom transfer radical polymerization. Science 332 (6025): 81–84.
107. Shida, N., Nishiyama, H., Tomita, I., Inagi, S. (2019). Layer-by-layer Multilayered Film Formation on Gradient Polyelectrolyte Brush Prepared by Bipolar Electrochemistry. Chemistry Letters 48 (9): 1174–1177.
108. Shida, N., Kitamura, F., Fuchigami, T., Tomita, I., Inagi, S. (2016). Signal-Amplified Analysis of Molecular Layers Prepared through Bipolar Electrochemistry. ChemElectroChem 3 (3): 465–471.
109. Bankiewicz, D., Vainio, E., Yrjas, P., Hupa, L., Lisak, G. (2020). Application of bipolar electrochemistry to accelerate dew point corrosion for screening of steel materials for power boilers. Fuel 265: 116886.
110. Zhou, Y., Kablan, A., Engelberg, D.L. (2020). Metallographic screening of duplex stainless steel weld microstructure with a bipolar electrochemistry technique. Materials Characterization 169: 110605.
111. Munktell, S., Nyholm, L., Björefors, F. (2015). Towards high throughput corrosion screening using arrays of bipolar electrodes. Journal of Electroanalytical Chemistry 747: 77–82.

112. Zhou, Y. and Engelberg, D.L. (2020). On the Application of Bipolar Electrochemistry to Characterise the Localised Corrosion Behaviour of Type 420 Ferritic Stainless Steel. Metals 10 (6): 794.
113. McWilliams, S., Flynn, C.D., McWilliams, J., Arnold, D.C., Wahyuono, R.A., Undisz, A, et al. (2019). Nanostructured Cu2O Synthesized via Bipolar Electrochemistry. Nanomaterials. 9 (12): 1781.
114. Hakimian, A., McWilliams, S., Ignaszak, A. (2019). ZnO Synthesized Using Bipolar Electrochemistry: Structure and Activity. Materials. 12 (3): 535.
115. Xu, D., Feng, X., Song, Y., Li, X., Zhang, J., Chen, S., et al. (2020). Fast growth of highly ordered porous alumina films based on closed bipolar electrochemistry. Electrochemistry Communications 119: 106822.
116. Mor, G.K., Shankar, K., Paulose, M., Varghese, O.K., Grimes, C.A. (2005). Enhanced Photocleavage of Water Using Titania Nanotube Arrays. Nano Letters 5 (1): 191–195.
117. Mor, G.K., Shankar, K., Paulose, M., Varghese, O.K., Grimes, C.A. (2006). Use of Highly-Ordered TiO2 Nanotube Arrays in Dye-Sensitized Solar Cells. Nano Letters 6 (2): 215–258.
118. Kulkarni, M., Mazare, A., Gongadze, E., Perutkova, S., Kralj-Iglic, V., Milosev, I., et al. (2015). Titanium nanostructures for biomedical applications. Nanotechnology 26 (6): 062002.
119. Roy, P., Berger, S., Schmuki, P. (2011). TiO2 Nanotubes: Synthesis and Applications. Angewandte Chemie International Edition 50 (13): 2904–2939.
120. Loget, G., So, S., Hahn, R., Schmuki, P. (2014). Bipolar anodization enables the fabrication of controlled arrays of TiO2 nanotube gradients. Journal of Materials Chemistry A 2 (42): 17740–17745.
121. Loget, G. and Schmuki, P. (2014). H2 Mapping on Pt-Loaded TiO2 Nanotube Gradient Arrays. Langmuir 30 (50): 15356–15363.
122. Saqib, M., Lai, J., Zhao, J., Li, S., Xu, G. (2016). Bipolar Electrochemical Approach with a Thin Layer of Supporting Electrolyte towards the Growth of Self-Organizing TiO2 Nanotubes. ChemElectroChem 3 (3): 360–365.
123. Li, Y., Wang, S., Dong, Y., Mu, P., Yang, Y., Liu, X., et al. (2020). Effect of size and crystalline phase of TiO2 nanotubes on cell behaviors: A high throughput study using gradient TiO2 nanotubes. Bioactive Materials 5 (4): 1062–1070.
124. Sopha, H., Hromadko, L., Motola, M., Macak, J.M. (2020). Fabrication of TiO2 nanotubes on Ti spheres using bipolar electrochemistry. Electrochemistry Communications 111: 106669.
125. Roche, J., Gianessi, E., Kuhn, A. (2014). Physico-chemical milling for controlled size reduction of metal beads. Physical Chemistry Chemical Physics 16 (39): 21234–21236.
126. Chow, K.-F., Chang, B.-Y., Zaccheo, B.A., Mavré, F., Crooks, R.M. (2010). A Sensing Platform Based on Electrodissolution of a Ag Bipolar Electrode. Journal of the American Chemical Society 132 (27): 9228–9229.
127. Fosdick, S.E., Berglund, S.P., Mullins, C.B., Crooks, R.M. (2013). Parallel Screening of Electrocatalyst Candidates Using Bipolar Electrochemistry. Analytical Chemistry 85: 2493–2499.
128. Naser-Sadrabadi, A., Zare, H.R., Benvidi, A. (2020). Photochemical deposition of palladium nanoparticles on TiO2 nanoparticles and their application for electrocatalytic measurement of nitrate ions in potato, onion and cabbage using bipolar electrochemical method. Measurement 166: 108222.
129. Beugré, R., Dorval, A., Lavallée, L.L., Jafari, M., Byers, J.C. (2019). Local electrochemistry of nickel (oxy)hydroxide material gradients prepared using bipolar electrodeposition. Electrochimica Acta 319: 331–338.
130. Sahu, O., Mazumdar, B., Chaudhari, P.K. (2014). Treatment of wastewater by electrocoagulation: a review. Environmental Science and Pollution Research 21 (4): 2397–2413.
131. Qi, Z.L., Zhang, J.N., You, S.J. (2018). Effect of placement angles on wireless electrocoagulation for bipolar aluminum electrodes. Frontiers of Environmental Science & Engineering. 12: 9.
132. Qi, Z., You, S., Ren, N. (2017). Wireless Electrocoagulation in Water Treatment Based on Bipolar Electrochemistry. Electrochimica Acta 229: 96–101.

133. Abdelkader, A.M., Cooper, A.J., Dryfe, R.A.W., Kinloch, I.A. (2015). How to get between the sheets: a review of recent works on the electrochemical exfoliation of graphene materials from bulk graphite. Nanoscale 7 (16): 6944–6956.
134. Hashimoto, H., Muramatsu, Y., Nishina, Y., Asoh, H. (2019). Bipolar anodic electrochemical exfoliation of graphite powders. Electrochemistry Communications 104: 106475.
135. Rabiei Baboukani, A., Khakpour, I., Drozd, V., Allagui, A., Wang, C. (2019). Single-step exfoliation of black phosphorus and deposition of phosphorene via bipolar electrochemistry for capacitive energy storage application. Journal of Materials Chemistry A 7 (44): 25548–25556.
136. Paxton, W.F., Sundararajan, S., Mallouk, T.E., Sen, A. (2006). Chemical Locomotion. Angewandte Chemie International Edition 45 (33): 5420–5429.
137. Wang, J. and Manesh, K.M. (2010). Motion Control at the Nanoscale. Small 6 (3): 338–345.
138. Wang, H. and Pumera, M. (2015). Fabrication of Micro/Nanoscale Motors. Chemical Reviews 115 (16): 8704–8735.
139. Bouffier, L., Ravaine, V., Sojic, N., Kuhn, A. (2016). Electric fields for generating unconventional motion of small objects. Current Opinion in Colloid & Interface Science 21: 57–64.
140. Xu, L., Mou, F., Gong, H., Luo, M., Guan, J. (2017). Light-driven micro/nanomotors: from fundamentals to applications. Chemical Society Reviews 46 (22): 6905–6926.
141. Ye, Y., Luan, J., Wang, M., Chen, Y., Wilson, D.A., Peng, F., et al. (2019). Fabrication of Self-Propelled Micro- and Nanomotors Based on Janus Structures. Chemistry – A European Journal 25 (37): 8663–8680.
142. Gao, W. and Wang, J. (2014). Synthetic micro/nanomotors in drug delivery. Nanoscale 6 (18): 10486–10494.
143. Peng, F., Tu, Y., Wilson, D.A. (2017). Micro/nanomotors towards in vivo application: cell, tissue and biofluid. Chemical Society Reviews 46 (17): 5289–5310.
144. Ying, Y. and Pumera, M. (2019). Micro/Nanomotors for Water Purification. Chemistry – A European Journal 25 (1): 106–121.
145. Paxton, W.F., Baker, P.T., Kline, T.R., Wang, Y., Mallouk, T.E., Sen, A. (2006). Catalytically Induced Electrokinetics for Motors and Micropumps. Journal of the American Chemical Society 128: 14881–14888.
146. Wang, Y., Hernandez, R.M., Bartlett, D.J., Bingham, J.M., Kline, T.R., Sen, A., et al. (2006). Bipolar Electrochemical Mechanism for the Propulsion of Catalytic Nanomotors in Hydrogen Peroxide Solutions Langmuir 22 (25): 10451–10456.
147. Paxton, W.F., Kistler, K.C., Olmeda, C.C., Sen, A., St. Angelo, S.K., Cao, Y., et al. (2004). Catalytic Nanomotors: Autonomous Movement of Striped Nanorods. Journal of the American Chemical Society 126 (41): 13424–13431.
148. Paxton, W.F., Sen, A., Mallouk, T.E. (2005). Motility of Catalytic nanoparticles through self-generated forces. Chemistry – A European Journal 11: 6462–6470.
149. Kline, T.R., Tian, M., Wang, J., Sen, A., Chan, M.W., Mallouk, T.E. (2006). Template-grown metal nanowires. Inorganic Chemistry 45 (19): 7555–7565.
150. Laocharoensuk, R., Burdick, J., Wang, J. (2008). Carbon-Nanotube-Induced Acceleration of Catalytic Nanomotors. ACS Nano 2 (5): 1069–1075.
151. Mei, Y., Huang, G., Solovev, A.A., Ureña, E.B., Mönch, I., Ding, F., et al. (2008). Versatile Approach for Integrative and Functionalized Tubes by Strain Engineering of Nanomembranes on Polymers. Advanced Materials 20 (21): 4085–4090.
152. Solovev, A.A., Sanchez, S., Pumera, M., Mei, Y.F., Schmidt, O.G. (2010). Magnetic Control of Tubular Catalytic Microbots for the Transport, Assembly, and Delivery of Micro-objects. Advanced Functional Materials 20 (15): 2430–2435.
153. Manesh, K.M., Cardona, M., Yuan, R., Clark, M., Kagan, D., Balasubramanian, S., et al. (2010). Template-Assisted Fabrication of Salt-Independent Catalytic Tubular Microengines. ACS Nano 4 (4): 1799–1804.

154. Mei, Y., Solovev, A.A., Sanchez, S., Schmidt, O.G. (2011). Rolled-up nanotech on polymers: from basic perception to self-propelled catalytic microengines. Chemical Society Reviews 40 (5): 2109–2119.
155. Gao, W., Sattayasamitsathit, S., Orozco, J., Wang, J. (2011). Highly Efficient Catalytic Microengines: Template Electrosynthesis of Polyaniline/Platinum Microtubes. Journal of the American Chemical Society 133 (31): 11862–11864.
156. Wang, W., Chiang, T.-Y., Velegol, D., Mallouk, T.E. (2013). Understanding the Efficiency of Autonomous Nano- and Microscale Motors. Journal of the American Chemical Society 135: 10557–10565.
157. Qin, L., Banholzer, M.J., Xu, X., Huang, L., Mirkin, C.A. (2007). Rational Design and Synthesis of Catalytically Driven Nanorotors. Journal of the American Chemical Society 129 (48): 14870–14871.
158. Fattah, Z., Loget, G., Lapeyre, V., Garrigue, P., Warakulwit, C., Limtrakul, J., et al. (2011). Straightforward single-step generation of microswimmers by bipolar electrochemistry. Electrochimica Acta 56 (28): 10562–10566.
159. Ibele, M.E., Wang, Y., Kline, T.R., Mallouk, T.E., Sen, A. (2007). Hydrazine Fuels for Bimetallic Catalytic Microfluidic Pumping. Journal of the American Chemical Society 129 (25): 7762–7763.
160. Liu, R. and Sen, A. (2011). Autonomous Nanomotor Based on Copper–Platinum Segmented Nanobattery. Journal of the American Chemical Society 133 (50): 20064–20067.
161. Gao, W., Feng, X., Pei, A., Gu, Y., Li, J., Wang, J. (2013). Seawater-driven magnesium based Janus micromotors for environmental remediation. Nanoscale 5 (11): 4696–4700.
162. Chen, C., Karshalev, E., Guan, J., Wang, J. (2018). Magnesium-Based Micromotors: Water-Powered Propulsion, Multifunctionality, and Biomedical and Environmental Applications. Small 14 (23): 1704252.
163. Salinas, G., Dauphin, A.L., Voci, S., Bouffier, L., Sojic, N., Kuhn, A. (2020). Asymmetry controlled dynamic behavior of autonomous chemiluminescent Janus microswimmers. Chemical Science 11 (28): 7438–7443.
164. Loget, G. and Kuhn, A. (2010). Propulsion of Microobjects by Dynamic Bipolar Self-Regeneration. Journal of the American Chemical Society 132 (45): 15918–15919.
165. Loget, G. and Kuhn, A. (2011). Electric field-induced chemical locomotion of conducting objects. Nature Communications 2: 535.
166. Jiang, J.-Z., Guo, M.-H., Yao, F.-Z., Li, J., Sun, J.-J. (2017). Propulsion of copper microswimmers in folded fluid channels by bipolar electrochemistry. RSC Advances 7 (11): 6297–6302.
167. Loget, G. and Kuhn, A. (2012). Bipolar electrochemistry for cargo-lifting in fluid channels. Lab on a Chip 12: 1967–1971.
168. Sentic, M., Loget, G., Manojlovic, D., Kuhn, A., Sojic, N. (2012). Light-Emitting Electrochemical “Swimmers”. Angewandte Chemie International Edition 51 (45): 11284–11288.
169. Bouffier, L., Zigah, D., Adam, C., Sentic, M., Fattah, Z., Manojlovic, D., et al. (2014). Lighting Up Redox Propulsion with Luminol Electrogenerated Chemiluminescence. ChemElectroChem 1: 95–98.
170. Sentic, M., Arbault, S., Goudeau, B., Manojlovic, D., Kuhn, A., Bouffier, L., et al. (2014). Electrochemiluminescent swimmers for dynamic enzymatic sensing. Chemical Communications 50 (71): 10202–10205.
171. Roche, J., Carrara, S., Lannelongue, J., Loget, G., Bouffier, L., Kuhn, A., et al. (2014). Wireless powering of e-swimmers. Scientific Reports 4: 6705.
172. Bouffier, L. and Kuhn, A. (2013). Design of a wireless electrochemical valve. Nanoscale 5 (4): 1305–1309.
173. Eßmann, V., Voci, S., Loget, G., Sojic, N., Schuhmann, W., Kuhn, A. (2017). Wireless Light-Emitting Electrochemical Rotors. The Journal of Physical Chemistry Letters 8 (19): 4930–4934.
174. Gupta, B., Goudeau, B., Garrigue, P., Kuhn, A. (2018). Bipolar Conducting Polymer Crawlers Based on Triple Symmetry Breaking. Advanced Functional Materials 28 (25): 1705825.

175. Gupta, B., Goudeau, B., Kuhn, A. (2017). Wireless Electrochemical Actuation of Conducting Polymers. Angewandte Chemie International Edition 56 (45): 14183–14186.
176. Gupta, B., Afonso, M.C., Zhang, L., Ayela, C., Garrigue, P., Goudeau, B., et al. (2019). Wireless Coupling of Conducting Polymer Actuators with Light Emission. ChemPhysChem 20 (7): 941–945.
177. Arora, A., Eijkel, J.C.T., Morf, W.E., Manz, A. (2001). A Wireless Electrochemiluminescence Detector Applied to Direct and Indirect Detection for Electrophoresis on a Microfabricated Glass Device. Analytical Chemistry 73 (14): 3282–3288.
178. Zhan, W., Alvarez, J., Crooks, R.M. (2002). A Two-Channel Microfluidic Sensor That Uses Anodic Electrogenerated Chemiluminescence as a Photonic Reporter of Cathodic Redox Reactions. Analytical Chemistry 75 (2): 313–318.
179. Zhan, W., Alvarez, J., Crooks, R.M. (2002). Electrochemical Sensing in Microfluidic Systems Using Electrogenerated Chemiluminescence as a Photonic Reporter of Redox Reactions. Journal of the American Chemical Society 124 (44): 13265–13270.
180. Bouffier, L., Doneux, T., Goudeau, B., Kuhn, A. (2014). Imaging Redox Activity at Bipolar Electrodes by Indirect Fluorescence Modulation. Analytical Chemistry 86: 3708–3711.
181. Xu, W., Fu, K., Ma, C., Bohn, P.W. (2016). Closed bipolar electrode-enabled dual-cell electrochromic detectors for chemical sensing. Analyst 141 (21): 6018–6024.
182. Zhai, Q., Zhang, X., Xia, Y., Li, J., Wang, E. (2016). Electrochromic sensing platform based on steric hindrance effects for CEA detection. Analyst 141 (13): 3985–3988.
183. Zhang, L., Gupta, B., Goudeau, B., Mano, N., Kuhn, A. (2018). Wireless Electromechanical Readout of Chemical Information. Journal of the American Chemical Society 140 (45): 15501–15506.
184. Zhan, W., Alvarez, J., Sun, L., Crooks, R.M. (2003). A multichannel microfluidic sensor that detects anodic redox reactions indirectly using anodic electrogenerated chemiluminescence. Anal Chem. Analytical Chemistry 75 (6): 1233–1238.
185. Zhan, W., Crooks, R.M. (2003). Microelectrochemical Logic Circuits. Journal of the American Chemical Society 125 (33): 9934–9935.
186. Chow, K.-F., Mavré, F., Crooks, R.M. (2008). Wireless Electrochemical DNA Microarray Sensor. Journal of the American Chemical Society 130 (24): 7544–7545.
187. Crooks, R.M. (2016). Principles of Bipolar Electrochemistry. ChemElectroChem 3 (3): 357–359.
188. Rahn, K.L., Rhoades, T.D., Anand, R.K. (2020). Alternating Current Voltammetry at a Bipolar Electrode with Smartphone Luminescence Imaging for Point-of-Need Sensing. ChemElectroChem 7 (5): 1172–1181.
189. Gao, W., Muzyka, K., Ma, X., Lou, B., Xu, G. (2018). A single-electrode electrochemical system for multiplex electrochemiluminescence analysis based on a resistance induced potential difference. Chemical Science 9 (16): 3911–3916.
190. Liu, Z., Qi, W., Xu, G. (2015). Recent advances in electrochemiluminescence. Chemical Society Reviews 44 (10): 3117–3142.
191. Mavré, F., Chow, K.-F., Sheridan, E., Chang, B.-Y., Crooks, J.A., Crooks, R.M. (2009). A Theoretical and Experimental Framework for Understanding Electrogenerated Chemiluminescence (ECL) Emission at Bipolar Electrodes. Analytical Chemistry 81 (15): 6218–6225.
192. Kostiuchenko, Z.A., Zhang, B., Lemay, S.G. (2016). Stochastic Charge Fluctuations in Bipolar Electrodes. The Journal of Physical Chemistry C 120 (40): 22777–22783.
193. He, D., Yan, J., Zhu, F., Zhou, Y., Mao, B., Oleinick, A., et al. (2016). Enhancing the Bipolar Redox Cycling Efficiency of Plane-Recessed Microelectrode Arrays by Adding a Chemically Irreversible Interferent. Analytical Chemistry 88 (17): 8535–8541.
194. Guerrette, J.P., Oja, S.M., Zhang, B. (2012). Coupled Electrochemical Reactions at Bipolar Microelectrodes and Nanoelectrodes. Analytical Chemistry 84 (3): 1609–1616.
195. Chow, K.-F., Mavré, F., Crooks, J.A., Chang, B.-Y., Crooks, R.M. (2009). A Large-Scale, Wireless Electrochemical Bipolar Electrode Microarray. Journal of the American Chemical Society 131 (24): 8364–8365.

196. Mavré, F., Anand, R.K., Laws, D.R., Chow, K.-F., Chang, B.-Y., Crooks, J.A., et al. (2010). Bipolar Electrodes: A Useful Tool for Concentration, Separation, and Detection of Analytes in Microelectrochemical Systems. Analytical Chemistry 82 (21): 8766–8774.
197. Chang, B.-Y., Chow, K.-F., Crooks, J.A., Mavré, F., Crooks, R.M. (2012). Two-channel microelectrochemical bipolar electrode sensor array. Analyst 137 (12): 2827–2833.
198. Oja, S.M. and Zhang, B. (2016). Electrogenerated Chemiluminescence Reporting on Closed Bipolar Microelectrodes and the Influence of Electrode Size. ChemElectroChem 3 (3): 457–464.
199. Chang, B.-Y., Mavré, F., Chow, K.-F., Crooks, J.A., Crooks, R.M. (2010). Snapshot Voltammetry Using a Triangular Bipolar Microelectrode. Analytical Chemistry 82 (12): 5317–5322.
200. Borchers, J.S., Riusech, O., Rasmussen, E., Anand, R.K. (2019). Visual Voltammogram at an Array of Closed Bipolar Electrodes in a Ladder Configuration. Journal of Analysis and Testing 3 (2): 150–159.
201. Hasheminejad, M., Fang, Y., Li, M., Jiang, Y., Wang, W., Chen, H.-Y. (2017). Plasmonic Imaging of the Interfacial Potential Distribution on Bipolar Electrodes. Angewandte Chemie International Edition 56 (6): 1629–1633.
202. Li, M., Liu, S., Jiang, Y., Wang, W. (2018). Visualizing the Zero-Potential Line of Bipolar Electrodes with Arbitrary Geometry. Analytical Chemistry 90 (11): 6390–6396.
203. Fosdick, S.E., Crooks, J.A., Chang, B.-Y., Crooks, R.M. (2010). Two-Dimensional Bipolar Electrochemistry. Journal of the American Chemical Society 132 (27): 9226–9227.
204. Sentic, M., Arbault, S., Bouffier, L., Manojlovic, D., Kuhn, A., Sojic, N. (2015). 3D electrogenerated chemiluminescence: from surface-confined reactions to bulk emission. Chemical Science 6: 4433–4437
205. de Poulpiquet, A., Diez-Buitrago, B., Milutinovic, M., Goudeau, B., Bouffier, L., Arbault, S., et al. (2016). Dual-Color Electrogenerated Chemiluminescence from Dispersions of Conductive Microbeads Addressed by Bipolar Electrochemistry. ChemElectroChem 3 (3): 404–409.
206. de Poulpiquet, A., Diez-Buitrago, B., Dumont Milutinovic, M., Sentic, M., Arbault, S., Bouffier, L., et al. (2016). Dual Enzymatic Detection by Bulk Electrogenerated Chemiluminescence. Analytical Chemistry 88 (12): 6585–6592.
207. Ding, S.-N., Wang, X.-Y., Lu, W.-X. (2019). Switches-controlled bipolar electrode electrochemiluminescence arrays for high-throughput detection of cancer biomarkers. Journal of Electroanalytical Chemistry 844: 99–104.
208. Khoshfetrat, S.M., Ranjbari, M., Shayan, M., Mehrgardi, M.A., Kiani, A. (2015). Wireless electrochemiluminescence bipolar electrode array for visualized genotyping of single nucleotide polymorphism. Analytical Chemistry 87 (16): 8123–8131.
209. Wu, M.-S., Liu, Z., Shi, H.-W., Chen, H.-Y., Xu, J.-J. (2016). Visual Electrochemiluminescence Detection of Cancer Biomarkers on a Closed Bipolar Electrode Array Chip. Analytical Chemistry 87 (1): 530–537.
210. Xiao, Y., Xu, L., Qi, L.-W. (2017). Electrochemiluminescence bipolar electrode array for the multiplexed detection of glucose, lactate and choline based on a versatile enzymatic approach. Talanta 165: 577–583.
211. Wu, M., Xu, N., Qiao, J., Chen, J., Jin, L. (2019). Bipolar electrode-electrochemiluminescence (ECL) biosensor based on a hybridization chain reaction. Analyst 144 (15) : 4633–4638.
212. Zhang, X., Li, J., Jia, X., Li, D., Wang, E. (2014). Full-Featured Electrochemiluminescence Sensing Platform Based on the Multichannel Closed Bipolar System. Analytical Chemistry 86 (11): 5595–5599.
213. Liu, C., Wang, D., Zhang, C. (2018). A novel paperfluidic closed bipolar electrode-electrochemiluminescence sensing platform: Potential for multiplex detection at crossing-channel closed bipolar electrodes. Sensors and Actuators B: Chemical 270: 341–352.
214. Ge, S., Zhao, J., Wang, S., Lan, F., Yan, M., Yu, J. (2018). Ultrasensitive electrochemiluminescence assay of tumor cells and evaluation of H2O2 on a paper-based closed-

bipolar electrode by in-situ hybridization chain reaction amplification. Biosensors and Bioelectronics 102: 411–417.
215. Renault, C., Scida, K., Knust, K.N., Fosdick, S.E., Crooks, R.M. (2013). Paper-Based Bipolar Electrochemistry. Journal of Electrochemical Science and Technology 4 (4): 146–152.
216. Feng, Q.-M., Pan, J.-B., Zhang, H.-R., Xu, J.-J., Chen, H.-Y. (2014). Disposable paper-based bipolar electrode for sensitive electrochemiluminescence detection of a cancer biomarker. Chemical Communications 50 (75): 10949–10951.
217. Chen, L., Zhang, C., Xing, D. (2016). Paper-based bipolar electrode-electrochemiluminescence (BPE-ECL) device with battery energy supply and smartphone read-out: A handheld ECL system for biochemical analysis at the point-of-care level. Sensors and Actuators B: Chemical 237: 308–317.
218. Liu, H., Zhou, X., Liu, W., Yang, X., Xing, D. (2016). Paper-Based Bipolar Electrode Electrochemiluminescence Switch for Label-Free and Sensitive Genetic Detection of Pathogenic Bacteria. Analytical Chemistry 88 (20): 10191–10197.
219. Zhang, X., Bao, N., Luo, X., Ding, S.-N. (2018). Patchy gold coated Fe3O4 nanospheres with enhanced catalytic activity applied for paper-based bipolar electrode-electrochemiluminescence aptasensors. Biosensors and Bioelectronics 114: 44–51.
220. Zhang, X., Zhai, Q., Xu, L., Li, J., Wang, E. (2016). Paper-based electrochemiluminescence bipolar conductivity sensing mechanism: A critical supplement for the bipolar system. Journal of Electroanalytical Chemistry 781: 15–19.
221. Wang, F., Fu, C., Huang, C., Li, N., Wang, Y., Ge, S., et al. (2020). Paper-based closed Au-Bipolar electrode electrochemiluminescence sensing platform for the detection of miRNA-155. Biosensors and Bioelectronics 150: 111917.
222. Wang, F., Liu, Y., Fu, C., Li, N., Du, M., Zhang, L., et al. (2021). Paper-Based Bipolar Electrode Electrochemiluminescence Platform for Detection of Multiple miRNAs. Analytical Chemistry 93 (3): 1702–1708.
223. Li, M. and Anand, R.K. (2019). Integration of marker-free selection of single cells at a wireless electrode array with parallel fluidic isolation and electrical lysis. Chemical Science 10 (5): 1506–1513.
224. Wu, M.-S., Xu, B.-Y., Shi, H.-W., Xu, J.-J., Chen, H.-Y. (2011). Electrochemiluminescence analysis of folate receptors on cell membrane with on-chip bipolar electrode. Lab on a Chip 11 (16): 2720–2724.
225. Shi, H.-W., Wu, M.-S., Du, Y., Xu, J.-J., Chen, H.-Y. (2014). Electrochemiluminescence aptasensor based on bipolar electrode for detection of adenosine in cancer cells. Biosensors and Bioelectronics 55: 459–463.
226. Wu, M.-S., Liu, Z., Xu, J.-J., Chen, H.-Y. (2016). Highly Specific Electrochemiluminescence Detection of Cancer Cells with a Closed Bipolar Electrode. ChemElectroChem 3 (3): 429–435.
227. Motaghi, H., Ziyaee, S., Mehrgardi, M.A., Kajani, A.A., Bordbar, A.-K. (2018). Electrochemiluminescence detection of human breast cancer cells using aptamer modified bipolar electrode mounted into 3D printed microchannel. Biosensors and Bioelectronics 118: 217–223.
228. Shi, H.-W., Zhao, W., Liu, Z., Liu, X.-C., Xu, J.-J., Chen, H.-Y. (2016). Temporal Sensing Platform Based on Bipolar Electrode for the Ultrasensitive Detection of Cancer Cells. Analytical Chemistry 88 (17): 8795–8801.
229. Wu, M.-S., Qian, G.-s., Xu, J.-J., Chen, H.-Y. (2012). Sensitive Electrochemiluminescence Detection of c-Myc mRNA in Breast Cancer Cells on a Wireless Bipolar Electrode. Analytical Chemistry 84 (12): 5407–5414.
230. Wu, M.-S., Yuan, D.-J., Xu, J.-J., Chen, H.-Y. (2013). Sensitive Electrochemiluminescence Biosensor Based on Au-ITO Hybrid Bipolar Electrode Amplification System for Cell Surface Protein Detection. Analytical Chemistry 85 (24): 11960–11965.
231. Li, H., Bouffier, L., Arbault, S., Kuhn, A., Hogan, C.F., Sojic, N. (2017). Spatially-resolved multicolor bipolar electrochemiluminescence. Electrochemistry Communications 77: 10–13.

232. Moghaddam, M.R., Carrara, S., Hogan, C.F. (2019). Multi-colour bipolar electrochemiluminescence for heavy metal ion detection. Chemical Communications 55 (8): 1024–1027.
233. Wang, Y.-Z., Ji, S.-Y., Xu, H.-Y., Zhao, W., Xu, J.-J., Chen, H.-Y. (2018). Bidirectional Electrochemiluminescence Color Switch: An Application in Detecting Multimarkers of Prostate Cancer. Analytical Chemistry 90 (5): 3570–3575.
234. Wang, Y.-Z., Zhao, W., Dai, P.-P., Lu, H.-J., Xu, J.-J., Pan, J., et al. (2016). Spatial-resolved electrochemiluminescence ratiometry based on bipolar electrode for bioanalysis. Biosensors and Bioelectronics 86: 683–689.
235. Wang, Y.-Z., Xu, C.-H., Zhao, W., Guan, Q.-Y., Chen, H.-Y., Xu, J.-J. (2017). Bipolar Electrode Based Multicolor Electrochemiluminescence Biosensor. Analytical Chemistry 89 (15): 8050–8056.
236. Defnet, P.A. and Zhang, B. (2020). Detection of Transient Nanoparticle Collision Events Using Electrochemiluminescence on a Closed Bipolar Microelectrode. ChemElectroChem 7 (1): 252–259.
237. Anderson, T.J., Defnet, P.A., Zhang, B. (2020). Electrochemiluminescence (ECL)-Based Electrochemical Imaging Using a Massive Array of Bipolar Ultramicroelectrodes. Analytical Chemistry 92 (9): 6748–6755.
238. Lin, X.M., Zheng, L.Y., Gao, G.M., Chi, Y.W., Chen, G.N. (2012). Electrochemiluminescence Imaging-Based High-Throughput Screening Platform for Electrocatalysts Used in Fuel Cells. Analytical Chemistry 84 (18): 7700–7707.
239. Zhai, Q., Zhang, X., Han, Y., Zhai, J., Li, J., Wang, E. (2016). A Nanoscale Multichannel Closed Bipolar Electrode Array for Electrochemiluminescence Sensing Platform. Analytical Chemistry 88 (1): 945–951.
240. Ino, K., Yaegaki, R., Hiramoto, K., Nashimoto, Y., Shiku, H. (2020). Closed Bipolar Electrode Array for On-Chip Analysis of Cellular Respiration by Cell Aggregates. ACS Sensors 5 (3): 740–745.
241. Guo, W., Lin, X., Yan, F., Su, B. (2016). Vertically Ordered Silica Mesochannel Modified Bipolar Electrode for Electrochemiluminescence Imaging Analysis. ChemElectroChem 3 (3): 480–486.
242. Wu, S.Z., Zhou, Z.Y., Xu, L.R., Su, B., Fang, Q. (2014). Integrating bipolar electrochemistry and electrochemiluminescence imaging with microdroplets for chemical analysis. Biosensors and Bioelectronics 53: 148–153.
243. Yu, S., Mehrgardi, M., Shannon, C. (2018). A bipolar electrochemical sensor with square wave excitation and ECL readout. Electrochemistry Communications 88: 24–28.
244. Qi, L., Xia, Y., Qi, W., Gao, W., Wu, F., Xu, G. (2016). Increasing Electrochemiluminescence Intensity of a Wireless Electrode Array Chip by Thousands of Times Using a Diode for Sensitive Visual Detection by a Digital Camera. Analytical Chemistry 88 (2): 1123–1127.
245. Ma, X., Qi, L., Gao, W., Yuan, F., Xia, Y., Lou, B., et al. (2019). A portable wireless single-electrode system for electrochemiluminescent analysis. Electrochimica Acta 308: 20–24.
246. Qi, W., Lai, J., Gao, W., Li, S., Hanif, S., Xu, G. (2014). Wireless Electrochemiluminescence with Disposable Minidevice. Analytical Chemistry 86 (18): 8927–8931.
247. Li, H., Garrigue, P., Bouffier, L., Arbault, S., Kuhn, A., Sojic, N. (2016). Double remote electrochemical addressing and optical readout of electrochemiluminescence at the tip of an optical fiber. Analyst 141: 4299–4304.
248. Hao, R., Fan, Y., Han, C., Zhang, B. (2017). Bipolar Electrochemistry on a Nanopore-Supported Platinum Nanoparticle Electrode. Analytical Chemistry 89 (23): 12652–12658.
249. Liu, J., Pham, P., Haguet, V., Sauter-Starace, F., Leroy, L., Roget, A., et al. (2012). Polarization-Induced Local Pore-Wall Functionalization for Biosensing: From Micropore to Nanopore. Analytical Chemistry 84 (7): 3254–3261.
250. Gao, R., Ying, Y.-L., Li, Y.-J., Hu, Y.-X., Yu, R.-J., Lin, Y., et al. (2018). A 30 nm Nanopore Electrode: Facile Fabrication and Direct Insights into the Intrinsic Feature of Single Nanoparticle Collisions. Angewandte Chemie International Edition 57 (4): 1011–1015.

251. Li, Y., Chen, C., Willems, K., Kerman, S., Lagae, L., Groeseneken, G., et al. (2017). Probing Local Potentials inside Metallic Nanopores with SERS and Bipolar Electrochemistry. Advanced Optical Materials 5 (15): 1600907.
252. Marken, F. (2017). Confining Nanopore Bipolar Electrochemical Processes to Give Pattern in Space and Time. ChemElectroChem 4 (9): 2137–2139.
253. Ying, Y.-L., Hu, Y.-X., Gao, R., Yu, R.-J., Gu, Z., Lee, .L.P., et al. (2018). Asymmetric Nanopore Electrode-Based Amplification for Electron Transfer Imaging in Live Cells. Journal of the American Chemical Society 140 (16): 5385–5392.
254. Liu, J., Hébert, C., Pham, P., Sauter-Starace, F., Haguet, V., Livache, T., et al. (2012). Electrochemically Induced Maskless Metal Deposition on Micropore Wall. Small 8 (9): 1345–1349.
255. Ismail, A., Voci, S., Pham, P., Leroy, L., Maziz, A., Descamps, L., et al. (2019). Enhanced Bipolar Electrochemistry at Solid-State Micropores: Demonstration by Wireless Electrochemiluminescence Imaging. Analytical Chemistry 91 (14): 8900–8907.
256. Voci, S., Ismail, A., Pham, P., Yu, J., Maziz, A., Mesnilgrente, F., et al. (2020). Wireless Enhanced Electrochemiluminescence at a Bipolar Microelectrode in a Solid-State Micropore. Journal of the Electrochemical Society 167 (13): 137509.
257. Wang, Y., Jin, R., Sojic, N., Jiang, D., Chen, H.-Y. (2020). Intracellular Wireless Analysis of Single Cells by Bipolar Electrochemiluminescence Confined in Nanopipette. Angewandte Chemie International Edition 59 (26): 10416–10420.
258. Guerrette, J.P., Percival, S.J., Zhang, B. (2013). Fluorescence Coupling for Direct Imaging of Electrocatalytic Heterogeneity. Journal of the American Chemical Society 135 (2): 855–861.
259. Jusková, P., Neužil, P., Manz, A., Foret, F. (2013). Detection of electrochemiluminescence from floating metal platelets in suspension. Lab on a Chip 13 (5): 781–784.
260. Eßmann, V., Clausmeyer, J., Schuhmann, W. (2017). Alternating current-bipolar electrochemistry. Electrochemistry Communications 75: 82–85.
261. Dauphin, A.L., Akchach, A., Voci, S., Kuhn, A., Xu, G., Bouffier, L., et al. (2019). Tracking Magnetic Rotating Objects by Bipolar Electrochemiluminescence. The Journal of Physical Chemistry Letters 10 (18): 5318–5324.
262. Salinas, G., Pavel, I.-A., Sojic, N., Kuhn, A. (2020). Electrochemistry-Based Light-Emitting Mobile Systems. ChemElectroChem 7 (24): 4853–4862.
263. Oja, S.M., Guerrette, J.P., David, M.R., Zhang, B. (2014). Fluorescence-Enabled Electrochemical Microscopy with Dihydroresorufin as a Fluorogenic Indicator. Analytical Chemistry 86 (12): 6040–6048.
264. Stefano, J.S., Conzuelo, F., Masa, J., Munoz, R.A.A., Schuhmann, W. (2020). Coupling electrochemistry with a fluorescence reporting reaction enabled by bipolar electrochemistry. Journal of Electroanalytical Chemistry 872: 113921.
265. Xu, W., Ma, C., Bohn, P.W. (2016) Coupling of Independent Electrochemical Reactions and Fluorescence at Closed Bipolar Interdigitated Electrode Arrays. ChemElectroChem 3 (3): 422–428.
266. Qin, X., Li, Z.-Q., Zhou, Y., Pan, J.-B., Li, J., Wang, K., et al. (2020). Fabrication of High-Density and Superuniform Gold Nanoelectrode Arrays for Electrochemical Fluorescence Imaging. Analytical Chemistry 92 (19): 13493–13499.
267. Oja, S.M., Zhang, B. (2014). Imaging Transient Formation of Diffusion Layers with Fluorescence-Enabled Electrochemical Microscopy. Analytical Chemistry 86 (24): 12299–12307.
268. Scida, K., Eden, A., Arroyo-Currás, N., MacKenzie, S., Satik, Y., Meinhart, C.D., et al. (2019). Fluorescence-Based Observation of Transient Electrochemical and Electrokinetic Effects at Nanoconfined Bipolar Electrodes. ACS Applied Materials & Interfaces 11 (14): 13777–13786.
269. Ma, C., Zaino L.P.III, Bohn, P.W. (2015). Self-induced redox cycling coupled luminescence on nanopore recessed disk-multiscale bipolar electrodes. Chemical Science 6 (5): 3173–3179.
270. Xing, H., Zhang, X., Zhai, Q., Li, J., Wang, E. (2017). Bipolar Electrode Based Reversible Fluorescence Switch Using Prussian Blue/Au Nanoclusters Nanocomposite Film. Analytical Chemistry 89 (7): 3867–3872.

271. Davies, C.D., Yoon, E., Crooks, R.M. (2017). Continuous Redirection and Separation of Microbeads by Faradaic Ion Concentration Polarization. ChemElectroChem 5 (6): 877–884.
272. Davies, C.D. and Crooks, R.M. (2020). Focusing, sorting, and separating microplastics by serial faradaic ion concentration polarization. Chemical Science 11 (21): 5547–5558.
273. Jaworska, E., Michalska, A., Maksymiuk, K. (2019). Self-Powered Cascade Bipolar Electrodes with Fluorimetric Readout. Analytical Chemistry 91 (24): 15525–15531.
274. Jaworska, E., Michalska, A., Maksymiuk, K. (2020). Implementation of a Chloride-selective Electrode into a Closed Bipolar Electrode System with Fluorimetric Readout. Electroanalysis 32 (4): 812–819.
275. Jansod, S., Cherubini, T., Soda, Y., Bakker, E. (2020). Optical Sensing with a Potentiometric Sensing Array by Prussian Blue Film Integrated Closed Bipolar Electrodes. Analytical Chemistry 92 (13): 9138–9145.
276. Jansod, S., Cuartero, M., Cherubini, T., Bakker, E. (2018). Colorimetric Readout for Potentiometric Sensors with Closed Bipolar Electrodes. Analytical Chemistry 90 (11): 6376–6379.
277. Rafatmah, E. and Hemmateenejad, B. (2019). Colorimetric and visual determination of hydrogen peroxide and glucose by applying paper-based closed bipolar electrochemistry. Microchimica Acta 186 (11): 684.
278. Zheng, Y.-T., Zhao, B.-S., Zhang, H.-B., Jia, H., Wu, M. (2020). Colorimetric aptasensor for fumonisin B1 detection by regulating the amount of bubbles in closed bipolar platform. Journal of Electroanalytical Chemistry 877: 114584.
279. Crouch, G.M., Oh, C., Fu, K., Bohn, P.W. (2019). Tunable optical metamaterial-based sensors enabled by closed bipolar electrochemistry. Analyst 144 (21): 6240–6246.
280. Wang, L., Lian, W., Liu, H. (2016). A Resettable Keypad Lock with Visible Readout Based on Closed Bipolar Electrochemistry and Electrochromic Poly(3-methylthiophene) Films. Chemistry – A European Journal 22 (14): 4825–4832.
281. Xu, W., Fu, K., Bohn, P.W. (2017). Electrochromic Sensor for Multiplex Detection of Metabolites Enabled by Closed Bipolar Electrode Coupling. ACS Sensors 2 (7): 1020–1026.
282. Yu, X., Liang, J., Yang, T., Gong, M., Xi, D., Liu, H. (2018). A resettable and reprogrammable keypad lock based on electrochromic Prussian blue films and biocatalysis of immobilized glucose oxidase in a bipolar electrode system. Biosensors and Bioelectronics 99: 163–169.
283. Zhai, Q., Fan, D., Zhang, X., Li, J., Wang, E. (2017). Dual-electrochromic bipolar electrode-based universal platform for the construction of various visual advanced logic devices. NPG Asia Materials 9: e421.
284. Zhang, X., Shang, C., Gu, W., Xia, Y., Li, J., Wang, E. (2016). A Renewable Display Platform Based on the Bipolar Electrochromic Electrode. ChemElectroChem 3 (3): 383–386.
285. Zhang, X., Zhang, L., Zhai, Q., Gu, W., Li, J., Wang, E. (2016). Self-Powered Bipolar Electrochromic Electrode Arrays for Direct Displaying Applications. Analytical Chemistry 88 (5): 2543–2547.
286. Zhang, X., Lazenby, R.A., Wu, Y., White, R.J. (2019). Electrochromic, Closed-Bipolar Electrodes Employing Aptamer-Based Recognition for Direct Colorimetric Sensing Visualization. Analytical Chemistry 91 (17): 11467–11473.
287. Fosdick, S.E. and Crooks, R.M. (2012). Bipolar Electrodes for Rapid Screening of Electrocatalysts. Journal of the American Chemical Society 134 (2): 863–866.
288. Fosdick, S.E., Berglund, S.P., Mullins, C.B., Crooks, R.M. (2014). Evaluating Electrocatalysts for the Hydrogen Evolution Reaction Using Bipolar Electrode Arrays: Bi- and Trimetallic Combinations of Co, Fe, Ni, Mo, and W. ACS Catalysis 4 (5): 1332–1339.
289. Assavapanumat, S., Gupta, B., Salinas, G., Goudeau, B., Wattanakit, C., Kuhn, A. (2019). Chiral platinum-polypyrrole hybrid films as efficient enantioselective actuators. Chemical Communications 55 (73): 10956–10959.

290. Wattanakit, C., Bon Saint Côme, Y., Lapeyre, V., Bopp, P.A., Heim, M., Yadnum, S., et al. (2014). Enantioselective recognition at mesoporous chiral metal surfaces. Nature Communications 5 (1): 3325.
291. Wattanakit, C., Yutthalekha, T., Asssavapanumat, S., Lapeyre, V., Kuhn, A. (2017). Pulsed electroconversion for highly selective enantiomer synthesis. Nature Communications 8 (1): 2087.
292. Butcha, S., Assavapanumat, S., Ittisanronnachai, S., Lapeyre, V., Wattanakit, C., Kuhn, A. (2021). Nanoengineered chiral Pt-Ir alloys for high-performance enantioselective electrosynthesis. Nature Communications 12 (1): 1314.
293. Arnaboldi, S., Gupta, B., Benincori, T., Bonetti, G., Cirilli, R., Kuhn, A. (2020). Absolute Chiral Recognition with Hybrid Wireless Electrochemical Actuators. Analytical Chemistry 92 (14): 10042–10047.